© 2017. Published by The Company of Biologists Ltd | Journal of Cell Science (2017) 130, 963-974 doi:10.1242/jcs.196709

RESEARCH ARTICLE

Nucleoporins NPP-10, NPP-13 and NPP-20 are required for HCP-4 nuclear import to establish correct centromere assembly

Jorge Ferreira[1,*,‡,§], Jeffrey H. Stear[2] and Harald Saumweber[1,*]

ABSTRACT

Centromeres form a chromosomal platform for the assembly of the kinetochores, which are required for orderly chromosome segregation. Assembly of both centromeres and kinetochores proceeds by a step-by-step mechanism that is regulated in time and space. It has been suggested that the regulated nuclear import of centromeric proteins is involved in this process. We show that the knockdown of nucleoporins NPP-10, NPP-13 and NPP-20 in *Caenorhabditis elegans* affects early steps in centromere formation and sister centromere resolution, and results in severe chromosomal defects in the early embryo. These phenotypes mirror the knockdown phenotype of HCP-4 (an ortholog of mammalian CENP-C), a key factor for centromere formation and inner kinetochore assembly. HCP-4 is present in the cytoplasm during interphase. It is imported into nuclei and assembled in centromeres during prophase. Following the knockdown of NPP-10, NPP-13 and NPP-20, HCP-4 remains in the cytosol throughout prophase due to stalled import. In prometaphase and later mitotic stages after breakdown of the nuclear envelope, HCP-4 is not incorporated into centromeres. These results indicate that correct timing of the availability of HCP-4 by nuclear import is essential.

KEY WORDS: Centromere, Mitosis, *C. elegans* embryo, Nucleoporins

INTRODUCTION

Correct segregation of chromosomes during mitosis and meiosis is crucial for the maintenance of genome stability and cell function. Centromeres are chromatin structures that specify where the spindle attachment sites, termed kinetochores, will form (Fukagawa and Earnshaw, 2014). Kinetochores are DNA-free protein complexes formed by hundreds of proteins. They are visible in electron micrographs as trilaminar structures, with the inner kinetochore facing the centromere and the outer kinetochore providing the spindle attachment sites, which are critical for correct chromosomal segregation during mitosis and meiosis (see reviews by Kitagawa, 2010; Yamagishi et al., 2014; Cheeseman, 2014).

Centromeric DNA required for kinetochore assembly is typically defined by repeated sequences decorated by specific epigenetic markers. In particular, centromere function is specified by the centromere-specific histone H3 variant CENP-A, which is present in active centromeres of all eukaryotic cells (Kitagawa, 2010; De Rop et al., 2012). CENP-A binding establishes a platform to which all other centromere and kinetochore proteins are successively recruited. During replication, centromeric chromatin segregates between both chromatids. Therefore, before mitosis, newly replicated centromeric DNA must replenish centromere-specific proteins to generate fully functional sister centromeres. Loading of CENP-A to centromeric DNA is mediated by the chaperone HJURP (Foltz et al., 2009) and is regulated by the conserved Mis18 complex. However, the Mis18 complex does not directly bind to CENP-A but is recruited by the Mis18-binding protein M18BP1, which interacts with CENP-C, a constitutive centromeric protein with DNA-binding activity (Saitoh et al., 1992). Further studies have identified other proteins that bind to centromeric DNA and are referred as the constitutive centrosome associated network (CCAN; Okada et al., 2006; Hori et al., 2008, 2013). Some of these proteins have a histone fold and may form a nucleosome-like complex (Takeuchi et al., 2014). Part of the CCAN may form the interface between the centromere and the kinetochore that assembles stepwise on top of centromeres.

Studies using cultured mammalian cells as well as model systems such as yeast, worms and flies have revealed many details concerning centromere composition and function. In particular, the exaggerated holocentric centromere in *Caenorhabditis elegans*, which extends the entire length of the chromosome, has provided a unique perspective into centromere organization. Despite its cytologically distinct architecture, the *C. elegans* centromere shares structural and functional similarities with monocentric centromeres, and many proteins that provide these functions are conserved (Buchwitz et al., 1999; Moore et al., 1999; Moore and Roth, 2001; Oegema et al., 2001; Maddox et al., 2007; reviewed by Kitagawa, 2010). At its base is the centromeric histone variant CENP-A, called holocentric protein 3 (HCP-3) in *C. elegans*. Following immunostaining of interphase nuclei, HCP-3 is detected at many chromosomal sites (Buchwitz et al., 1999), and chromosome immunoprecipitation (ChIP) on chip analyses have revealed that HCP-3 occupies transcriptionally silent non-repeated DNA regions of 10-12 kb that are dispersed in the genome (Gassmann et al., 2012; Steiner and Henikoff, 2014). In prophase, the dispersed HCP-3 centromere seeds line up, forming an immature centromere along the condensing sister chromatids that later resolves into two centromeres facing the opposite sides of the paired sister chromatids in late prophase (Fig. 1). Loading of HCP-3 depends on KNL-2, the *C. elegans* homolog of M18BP1 (Maddox et al., 2007); in its absence, no HCP-3 is loaded and, conversely, KNL-2 is not chromosomally bound in nuclei that lack HCP-3.

The CENP-C homolog, HCP-4, is one of the earliest centromeric markers in *C. elegans*. A role in loading of HCP-3 to the centromere

[1]Cytogenetics group, Institute of Biology, Humboldt–Universität zu Berlin, Chausseestr. 117, Berlin 10115, Germany. [2]University of New South Wales, School of Medical Sciences, Sydney, New South Wales 2052, Australia.
*Present address: Humboldt University Berlin, Institute of Biology, Molecular Genetics, Philippstr. 11-13, Berlin 10115, Germany. ‡Present address: Department of Anesthesiology and Intensive Care Therapy, University Hospital Carl Gustav Carus, Dresden University of Technology, Dresden, Germany.

§Author for correspondence (jorgeferreira27@gmail.com)

J.F., 0000-0002-1972-0353

Received 16 August 2016; Accepted 13 January 2017

Journal of Cell Science (2017) 130, 963-974 doi:10.1242/jcs.196709

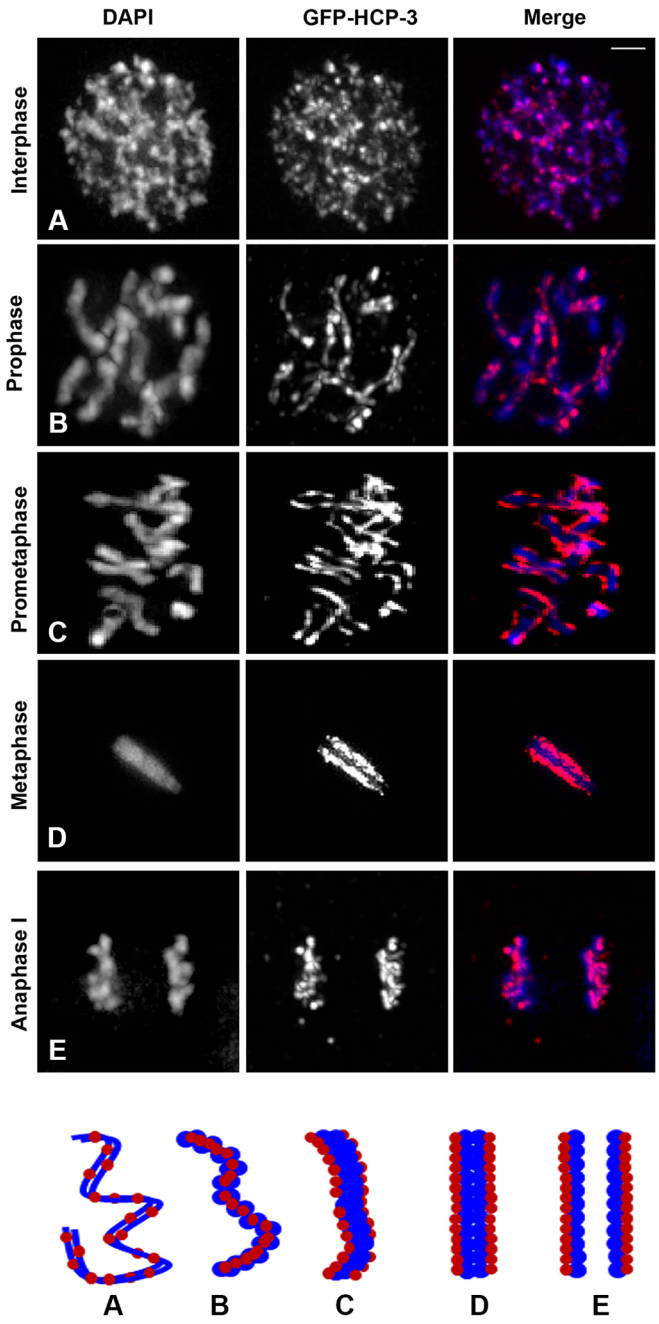

Fig. 1. Centromere formation in *C. elegans* two-cell embryos. Fixed two-cell embryos of a strain transgenic for GFP–HCP-3 were stained for GFP with antibodies using indirect immunofluorescence; DNA was stained by DAPI and data were recorded using image restoration microscopy. Data are displayed as a projection of stacks of deconvolved images. Single channels are in gray scale for DAPI and GFP–HCP-3, indicated at the top; merge: GFP–HCP-3 (red), DAPI (blue). (A) Interphase, (B) prophase, (C) prometaphase, (D) metaphase, (E) anaphase. Scale bar: 4 µm. Bottom: Schematic drawing of chromosomes corresponding to the micrographs A-E as indicated; HCP-3 red, DNA blue.

has not been established for HCP-4 (Maddox et al., 2007), as for its homolog CENP-C in vertebrates. However, HCP-4 is required for the formation of a functional centromere early on. Sister centromere resolution during late prophase takes place independent of spindle microtubules (Moore et al., 2005), indicating that spindle forces are not required for this process. However, in the absence of HCP-4, sister centromere resolution fails to occur, resulting in aberrant kinetochore formation, erroneous spindle assembly and severe chromosome segregation defects (Moore and Roth, 2001; Oegema et al., 2001). The role of HCP-4 in centromere resolution is still unclear. There is evidence for a function of HCP-4 in the removal of centromere cohesion (Moore et al., 2005). HCP-4 also bridges the centromere to kinetochore assembly. It is required for binding of KNL-1 (Desai et al., 2003), and both proteins cooperate in recruiting the CENP-F homolog HCP-1, the mitotic checkpoint kinase Bub1 and the microtubule depolymerizing kinesin KLP-7, also known as CeMCAK, in *C. elegans* to direct the assembly of the microtubule-binding interface of the kinetochore (Moore and Roth, 2001; Oegema et al., 2001; Desai et al., 2003).

The assembly of the centromere and the kinetochore is a precisely timed self-assembly process that is in synchrony with the cell cycle and therefore requires reliable spatial and temporal controls. One level of control affects protein stability through regulated proteolysis. Following APC-triggered proteasomal degradation of securin, separase is activated for condensin degradation, which in turn is essential for sister chromosome resolution (Yanagida, 2005). Similarly, several kinetochore components are degraded at the end of mitosis following ubiquitin ligation mediated by APC. The kinetochore protein CENP-I is modified and targeted for degradation by sumoylation (Gascoigne and Cheeseman, 2011). On the other hand, regulation through changes in gene expression does not appear to be an important mechanism for controlled centromere assembly since several constitutively expressed GFP-tagged versions of kinetochore proteins have an identical distribution to that of their endogenous counterparts (Gascoigne and Cheeseman, 2011). However, post-translational modification is a potent mechanism for timing the activity of proteins of the centromere-kinetochore complex. An attractive mechanism for coupling cell cycle regulation with centromere/kinetochore activity is phosphorylation by cell cycle-dependent kinases (Gascoigne and Cheeseman, 2011; McKinley and Cheeseman, 2014). Adding or removing sumoylation also influences the properties of many centromeric and kinetochore proteins without guiding them to degradation (reviewed by Wan et al., 2012).

Finally, the activity of centromeric proteins might be controlled by regulated import through the nuclear pore complexes (NPCs). Import restrictions could be selectively released through modifications of one of the ∼30 nucleoporins (Nups) making up the NPC (Raices and D′Angelo, 2012). Alternatively, proteins may pass through the nuclear pores only after they have been marked by specific post-translational modifications. Moreover, proteins could gain access to the nuclear compartment following nuclear envelope breakdown at prometaphase (Gascoigne and Cheeseman, 2011). The proteins of nuclear pore complexes are conserved between species, and 20 conserved nucleoporins (NPP-1 to NPP-20) have been identified in *C. elegans* (Galy et al., 2003). Some of these have been tested for their specific functions by using RNA interference (RNAi)-mediated knockdown in early *C. elegans* embryos (Galy et al., 2003; Schetter et al., 2006; Ródenas et al., 2009, 2012; Hajeri et al., 2010; Hachet et al., 2012; Ikegami and Lieb, 2013). Here, we have tested several nuclear pore proteins (NPPs) in *C. elegans* with respect to their contribution to centromere formation. Using RNAi knockdown, we found that the NPP-10 N- and C-terminal domains, NPP-13 and NPP-20 are required for the resolution of sister centromeres in prophase, similar to HCP-4. We show here that upon loss of any of these nucleoporins, HCP-4 is not imported into prophase nuclei. The lack of HCP-4 incorporation into the centromere is not corrected following nuclear envelope

Journal of Cell Science (2017) 130, 963-974 doi:10.1242/jcs.196709

breakdown in prometaphase, suggesting that correctly timing the availability of HCP-4 by nuclear import is essential for centromere/kinetochore assembly.

RESULTS

NPP knockdown strongly affects mitosis in early *C. elegans* embryos

To study the dynamic organization of centromeres in *C. elegans* embryos during the early stages of mitosis, we used immunofluorescence microscopy on fixed preparations or live-cell GFP imaging. For this purpose, we established a worm strain stably expressing GFP–HCP-3 and used a transgenic strain expressing GFP-tagged KNL-2 (Maddox et al., 2007). In fixed one- to two-cell embryos, GFP–HCP-3 displayed a spotted nuclear distribution during interphase (Fig. 1A), as reported previously (Buchwitz et al., 1999). During prophase, GFP–HCP-3 formed a single-line immature centromere associated with the condensing chromosomes (Fig. 1B). Later during prophase, GFP–HCP-3 centromeric staining resolved into two distinct lateral bands along each chromosome (Fig. 1C). This transition represents the centromere resolution along sister chromatids (Moore and Roth, 2001).

Throughout metaphase, the centromeres of all chromosomes were aligned on the poleward faces of the metaphase plate (Fig. 1D). Later, during anaphase, single centromeres stayed associated with the separating sister chromatids (Fig. 1E). Cartoons corresponding to the merged images of the micrographs in Fig. 1A-E are shown at the bottom of the figure. Very similar observations were made when we used GFP–KNL-2 as a marker (Fig. S1). Live-cell imaging of embryos allowed us to directly visualize the dynamic centromere organization in an interval of 2-3 min, as shown in Fig. S1 and Movies 1, 2.

Previously, *C. elegans* NPPs have been found to be essential for early development. RNAi knockdown of NPP genes causes severe defects in nuclear morphology (Galy et al., 2003). To address the potential role of nucleoporins in centromere function during M-phase, we used RNAi to deplete nucleoporins from *C. elegans* embryos. Of the 20 *C. elegans* nucleoporin genes, we selected six genes: *npp-7*/*NUP153*, *npp-8*/*NUP155*, *npp-10*/*NUP98* (encoding the Nup98-Nup96 precursor in mammals), *npp-13*/*NUP93*, *npp-19*/*NUP32* and *npp-20*/*SEC13R* (Galy et al., 2003; the mammalian orthologs are given). *npp-10* encodes a large precursor protein that is proteolytically cleaved to form an N-terminal domain (NPP-10N; an ortholog of mammalian Nup98) and a C-terminal domain (NPP-10C; an ortholog of mammalian Nup96). Since *npp-10* RNAi is targeted to the mRNA encoding the precursor for both protein products, it was designated as NPP-10 knockdown.

To test the efficiency of the NPP-targeting double-stranded (ds) RNAs under our conditions, we determined the survival rate of the progeny of treated animals. Similar to Galy et al. (2003), we found a significant rate of lethality between 98.6 and 99% for the dsRNA constructs used (Table 1). Following RNAi, all affected NPPs resulted in lethality. Embryos stopped development at a 50- to 100-cell stage and did not enter gastrulation. As shown by western blotting in Fig. 2A for *npp-7* RNAi, *npp-10* RNAi and *npp-13* RNAi embryos, the protein knockdown efficiency was estimated to be between 70 and 80%. Note, for *npp-10* RNAi, only knockdown of NPP-10N could be assessed due to the lack of specific antiserum against NPP-10C; antiserum was also unavailable for NPP-20. However, since NPP-10N and NPP-10C originate from a common RNAi target RNA encoding a precursor protein that is processed autocatalytically into both protein forms, we assume that both proteins were affected to similar extents by the knockdown (see Discussion). The knockdown was specific since NPP-10N was not significantly affected by unrelated *npp-20* or *npp-13* RNAi and, vice versa, NPP-13 was unaffected by *npp-20*- or *npp-10* RNAi knockdown. Efficient knockdown was also documented by the lack of immunostaining of the RNAi-treated embryos (Fig. 2B). In general, the knockdown of a given NPP did not strongly affect the distribution of the other NPPs, as shown for *npp-13* RNAi (Fig. 2C, lower). However, following *npp-10* knockdown, the nuclear pore distribution during prophase appeared patchy, indicating irregular clustering of nuclear pores (Fig. 2C, upper). Interestingly, knockdown of each of the six NPPs investigated resulted in strongly aberrant mitotic divisions. *npp-13*- and *npp-20* RNAi embryos showed a kinetochore-null-like (KNL) phenotype with aberrant mitotic behavior evident, already at mitotic prophase (Fig. S2; Movie 5). *npp-10* RNAi embryos also showed strong defects in chromosome condensation already at mitotic prophase (Fig. S2; Movie 4). *npp-7*, *npp-8* and *npp-19* RNAi embryos, on the other hand, formed relatively normal prometaphase and metaphase structures (Movies 3, 6) but showed aberrations at later mitotic stages (Fig. 3, see below).

Table 1. Early embryonic lethality following RNAi of nucleoporins

C. elegans nucleoporin genes[1]	Mammalian protein homologues[1]	Embryonic lethality (%)
npp-7	Nup153	99.0±0.4% (*n*=355)
npp-8	Nup155	98.8±0.4% (*n*=370)
npp-10	Nup98 and Nup96	99.0±0.4% (*n*=370)
npp-13	Nup93	98.6±0.8% (*n*=300)
npp-19	Nup35	99.0±0% (*n*=326)
npp-20	Sec13R	99.0±0.5% (*n*=380)

[1] Nomenclature used according to that of Galy et al. (2003).

Knockdown of NPP-10, NPP-13 and NPP-20 affects correct centromere assembly and resolution

Upon inspecting the knockdown effects of *npp-7*, *npp-8* and *npp-19* RNAi in detail, we found that prophase and prometaphase chromosomes formed paired sister centromeres (Fig. 3B-D). Although the line pattern of the centromeres following RNAi was more patchy, it was still similar to that of wild-type chromosomes (Fig. 3A). However, anaphase was aberrant in such animals (Fig. 3F-H; compare with Fig. 3E; see Movies 3, 6). In contrast, the knockdown of *npp-10*, *npp-13* or *npp-20* caused a severe failure in centromere assembly already in pro- and prometaphase, a failure that persisted during the remainder of the cell cycle. During prometaphase, when the nuclear envelope broke down, immature centromeres still remained as disrupted single-line structures and sister centromere resolution did not occur (Fig. 4B-D) with the typical double-line pattern that was seen in control embryos (Fig. 4A) and in *npp-7* RNAi-treated embryos (Fig. 4E). Since we sometimes observed pairs of dots on opposite sides of prometaphase chromosomes in RNAi-treated embryos, we cannot fully exclude the possibility of localized centromere resolution.

A quantitative evaluation of these effects is shown in Fig. 4F,G and in Table S1. Briefly, we randomly selected the same number of GFP–HCP-3- or GFP–KNL-2-stained two-cell embryos in prometaphase from the wild type and each NPP-knockdown condition. From each embryo, we counted the number of cytologically analyzable chromosomes showing sister centromere resolution (double-line centromeres) or not (single-line centromeres). The number of chromosomes found in each class was expressed as percent of the total analyzable chromosomes and is displayed in Fig. 4 and

Journal of Cell Science (2017) 130, 963-974 doi:10.1242/jcs.196709

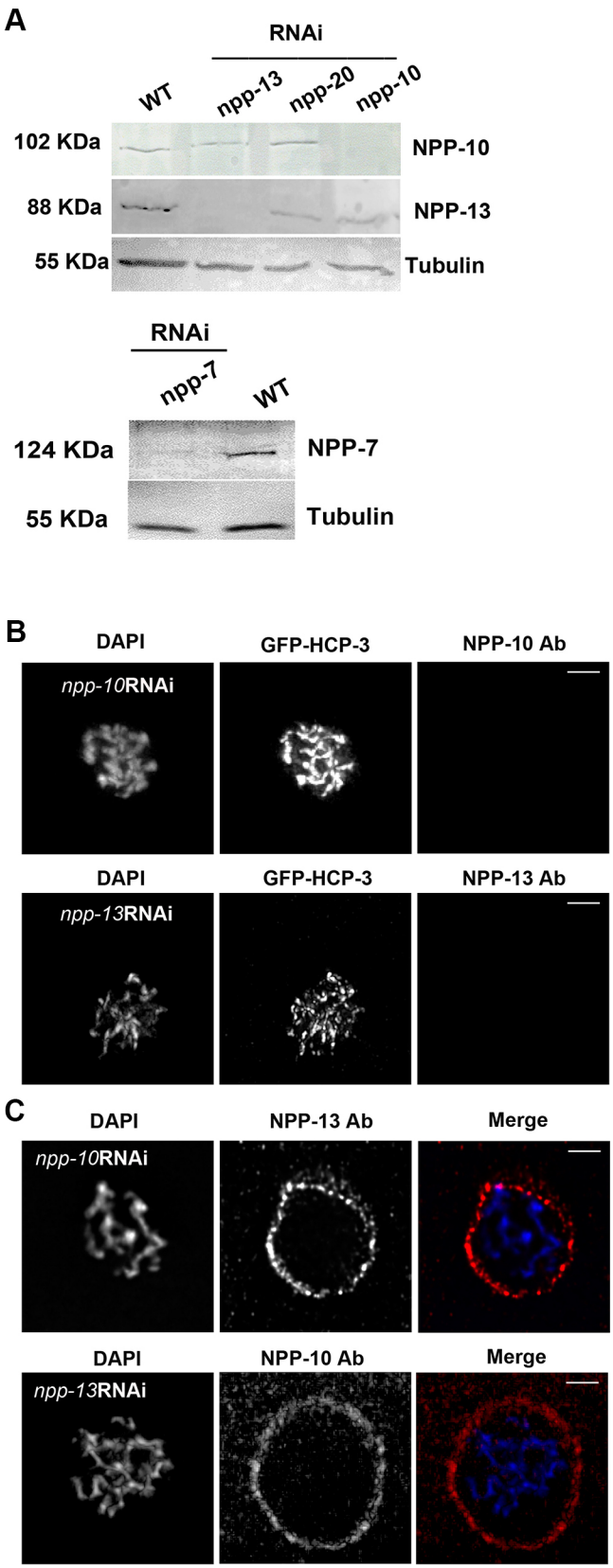

Fig. 2. NPP knockdown efficiency and specificity. RNAi knockdown was performed using the soaking method as described in Materials and Methods. (A) Western blot using cell extracts of wild-type (WT) controls and NPP-RNAi knockdown embryos, as indicated. Blots were tested with antisera against NPP-7, NPP-10N and NPP-13 or against tubulin as a loading control. The extent of knockdown was estimated by comparing the signal intensity of a specific band in wild-type and knockdown animals (n=4), both corrected using the loading control; note that following NPP-20 knockdown, neither NPP-10 nor NPP-13 was affected. (B) Double immunostaining of fixed prophase nuclei of GFP–HCP-3 transgenic embryos following *npp-10* RNAi (upper) or *npp-13* RNAi treatment (lower three panels). Nuclei were stained with anti-GFP and anti-NPP-10N antisera (upper) or with anti-GFP and anti-NPP-13 antisera (lower three panels); DNA was stained with DAPI. Staining of NPPs was undetectable in both cases. (C) Double immunostaining of fixed prophase nuclei of GFP–HCP-3 transgenic embryos following *npp-10* RNAi (upper) or *npp-13* RNAi (lower three panels). Nuclei were stained with anti-NPP-13 (upper) or anti-NPP-10N antisera (lower three panels); DNA was stained with DAPI. Note that NPP staining was clearly visible in both cases. All micrographs are displayed as projections of stacks of deconvolved images. Ab, antibody. Scale bars: 4 µm.

Table S1. Using GFP–HCP-3 as a marker for centromeres in cells that had been depleted of NPPs, we observed that only 17% (*npp-10* RNAi), 38% (*npp-13* RNAi) and 36% (*npp-20* RNAi) of the chromosomes resolved their centromeres and formed a double-line pattern. In contrast, the majority of chromosomes of control embryos (97%) and of NPP-7-depleted embryos (86%) exhibited centromere resolution (Fig. 4F; Table S1A). 60–70% of *npp-10*, *npp-13* or *npp-20* RNAi-treated embryos maintained immature single-line centromeres at this mitotic stage compared to 4% in wild type or 14% in *npp-7* RNAi-treated embryos, respectively (Fig. 4G; Table S1A). Quantification using GFP–KNL-2 as a centromeric marker showed similar results (Table S1). This effect was nucleoporin-specific since the knockdown of *npp-8* and *npp-19*, like the knockdown of *npp-7*, did not disrupt centromere maturation (Table S1A), although it strongly affected chromosome organization on the mitotic spindle during anaphase (Fig. 3). In conclusion, depletion of a subset of nucleoporins, NPP-10, NPP-13 and NPP-20, but not of NPP-7, NPP-8 and NPP-19, disrupts proper centromere resolution and sister chromatid segregation.

Knockdown of NPP-10, NPP-13 and NPP-20 affects nuclear import and centromere binding of HCP-4

Next, we sought to understand the role of NPP-10, NPP-13 and NPP-20 in the assembly of a functional centromere. The observed common effects of the knockdown of these three NPPs point to an early defect in the assembly and maturation of HCP-3 at the centromere. KNL-2 and HCP-4 are two proteins important at this early step of HCP-3 centromere assembly. In animals lacking KNL-2, no binding of HCP-3 to centromeres takes place, and no HCP-3 is incorporated into chromatin (Maddox et al., 2007). In contrast, disruption of HCP-4 does not affect HCP-3 binding but results in the assembly of immature centromeres and defects in sister chromatid resolution (Moore and Roth, 2001), similar to the phenotype we observed following NPP-10, NPP-13 and NPP-20 knockdown. Given that HCP-4 is mainly localized to the cytoplasm during interphase and is imported into the nucleus during prophase, we hypothesized that the knockdown of NPP-10, NPP-13 or NPP-20 might affect HCP-4 nuclear import.

During interphase, HCP-4 displayed a granular cytoplasmic pattern in wild type, as shown previously (Moore and Roth, 2001), with a small fraction also present within nuclei. HCP-4 distribution in embryos that had been treated with dsRNA against *npp-7*, *npp-10*, *npp-13* or *npp-20* was not significantly different from that in control embryos at this stage (data not shown). In control embryos during prophase, HCP-4 was imported into nuclei and recruited to sites along the axis of the chromosomes, forming immature single-line centromeres (Fig. 5A), which later resolve into the two sister

Journal of Cell Science (2017) 130, 963-974 doi:10.1242/jcs.196709

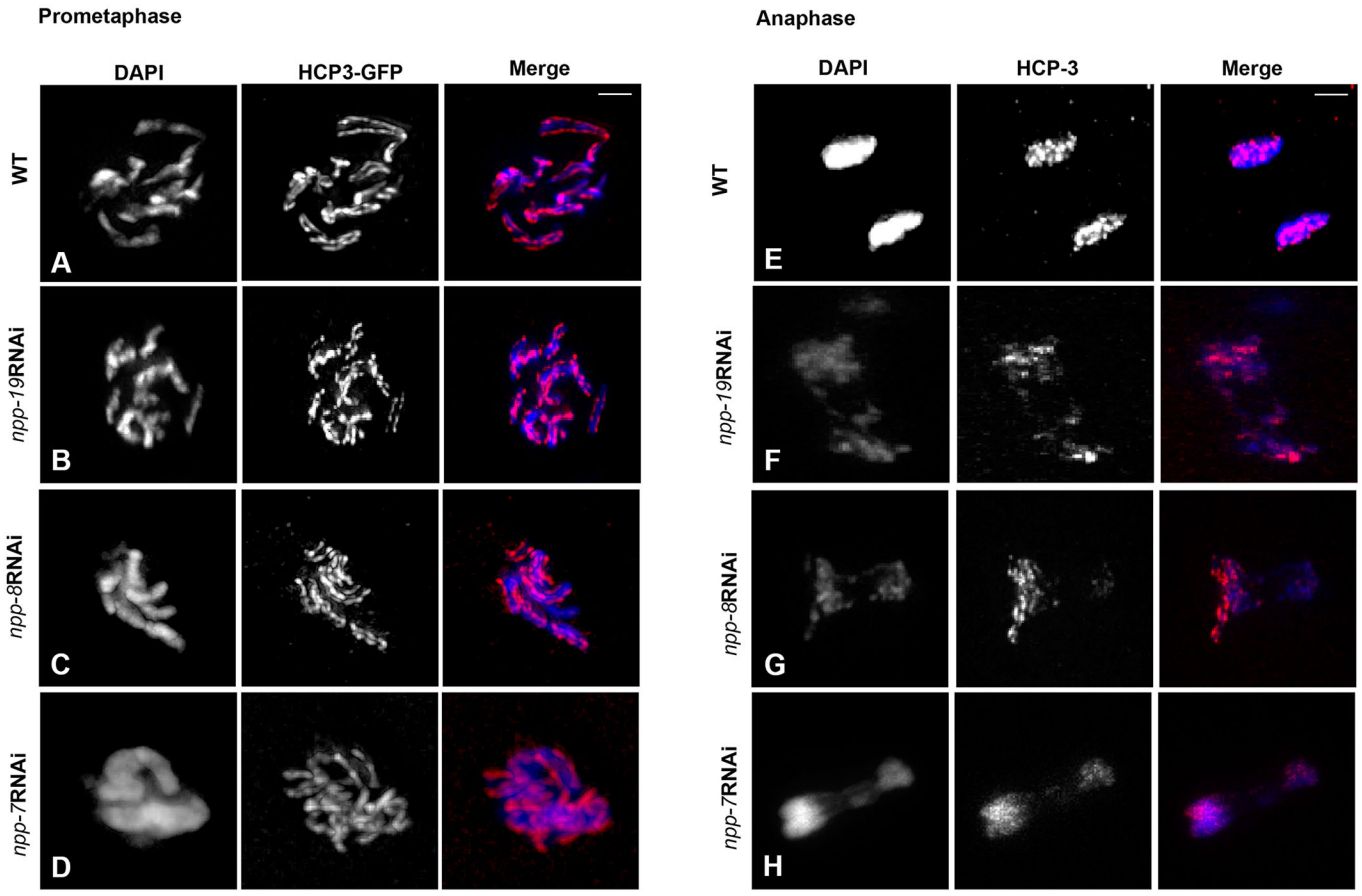

Fig. 3. RNAi knockdown of NPP-7, NPP-8 and NPP-19 results in defective anaphase resolution. Fixed GFP–HCP-3 transgenic two-cell embryos, treated with RNAi or untreated controls (wild type, WT), were immunostained with GFP-specific antibodies. DNA was stained by DAPI and data were recorded as described previously. Data are displayed as a projection of stacks of deconvolved images. Single channels for DAPI and GFP–HCP-3 are shown in gray scale. Merge: GFP–HCP-3, red; DAPI, blue. (A-D) Prometaphase; (E-H) anaphase; from top to bottom (A,E) WT control; (B,F) *npp-19* RNAi; (C,G) *npp-8* RNAi; (D-H) *npp-7* RNAi. Scale bars: 4 µm.

centromeres. Interestingly, HCP-4 was excluded from the nucleus to a significant extent in prophase cells that had been depleted of NPP-10 (Fig. 5B). HCP-4 remained in the cytosolic compartment, often with a conspicuous enrichment in the immediate nuclear environment (Fig. 5B). The nuclear exclusion of HCP-4 in prophase of *npp-10* RNAi animals is evident by co-staining of the nuclear envelope with lamin antibodies (Fig. 5F,G) and is in strong contrast to its nuclear enrichment in wild-type prophase nuclei (Fig. 5D,E). In contrast, in *npp-7* RNAi embryos, HCP-4 was imported into the nucleus, where it colocalized with GFP–HCP-3 protein (Fig. 5C), similar to in the wild-type controls (Fig. 5A). Like NPP-10 depletion, *npp-13* and *npp-20* RNAi knockdown resulted in a nuclear exclusion of HCP-4 (Fig. S3E,F). To quantify the observed HCP-4 depletion, we determined the ratio of HCP-4 in the nuclear compartment compared to that in the cytoplasmic compartment in wild-type and RNAi-knockdown animals. Embryos were double-stained for HCP-4 and the nuclear pore complex [using monoclonal antibody (MAb) 414], and five randomly chosen prophase embryos were evaluated for each condition. The mean intensity of HCP-4 staining in the nuclear (delineated by MAb414) and the adjacent cytoplasmic region was determined and displayed as the ratio of the nuclear-to-cytoplasmic staining normalized to the cytoplasmic staining for all animals of a given condition (Fig. 5H; Table S2; for details see Materials and Methods). The ratio value of 1.32 (import efficiency=100%) determined for wild type contrasted with a nuclear-to-cytoplasmic ratio of 0.40 (import efficiency=30.3%) obtained for *npp-10* RNAi- and a value of 0.55 (import efficiency=41.7%) for *npp-13* RNAi-treated animals, indicating a significant nuclear HCP-4 depletion due to defective import.

There was no HCP-4 recruitment to chromosomes in cells that had been depleted of HCP-3. HCP-4 remained mainly dispersed in the cytoplasm (Fig. S3B,I), as reported previously (Moore and Roth, 2001). In contrast, initial recruitment of GFP–HCP-3 (Fig. S3C,J) and GFP–KNL-2 (data not shown) to the centromere was unaffected by HCP-4 depletion. However, in these cells, chromosomes displayed an abnormal condensed morphology and did not undergo centromere resolution, as has been shown previously (Moore and Roth, 2001). In conclusion, NPP-10, NPP-13 and NPP-20 are required for nuclear import of HCP-4 during prophase to mediate the correct resolution of the immature centromere.

Following a critical phase, HCP-4 fails to be incorporated into centromeres

Since later in prometaphase the nuclear envelope breaks down and the chromosomes become accessible to HCP-4, we wondered whether HCP-4 may then become incorporated into centromeres, as seen in wild-type controls (Fig. 6A). However, upon NPP-10 knockdown, this was not the case (Fig. 6B). Although HPC-4 clearly was present in the former nuclear space, it did not incorporate significantly into centromeres but remained outside and in between the chromosomes.

Journal of Cell Science (2017) 130, 963-974 doi:10.1242/jcs.196709

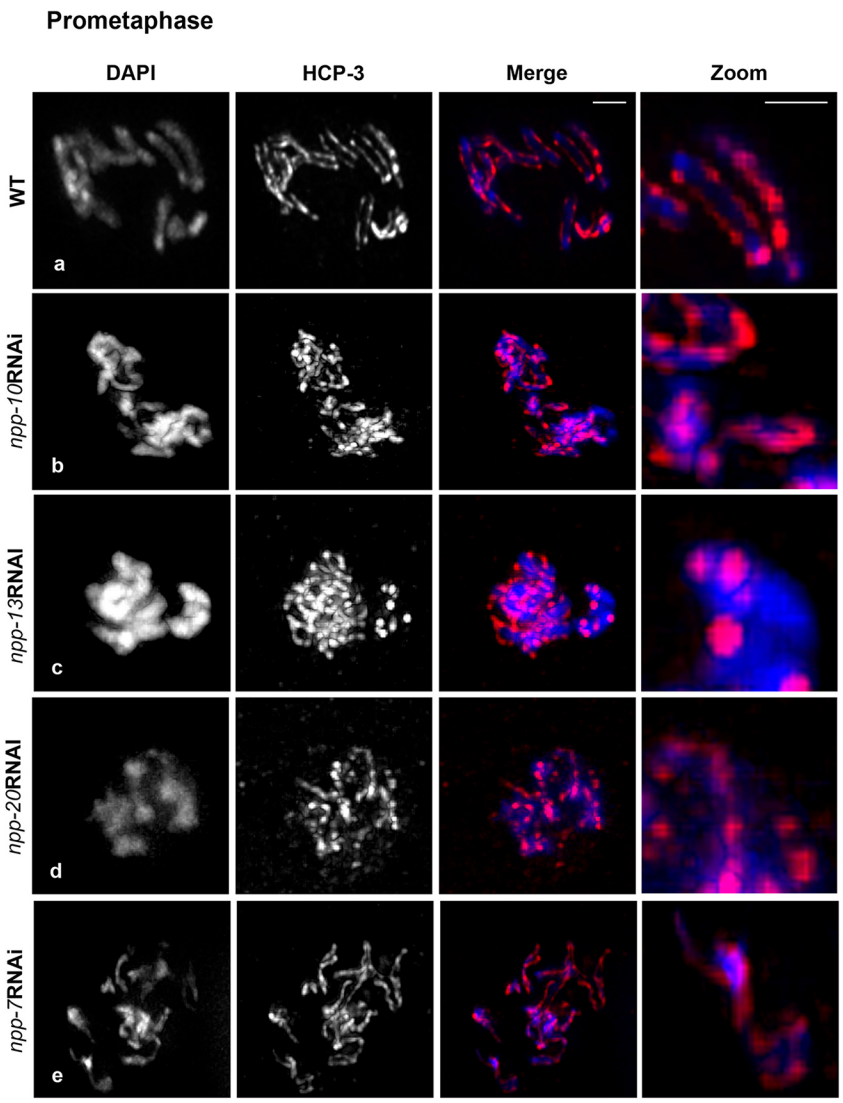

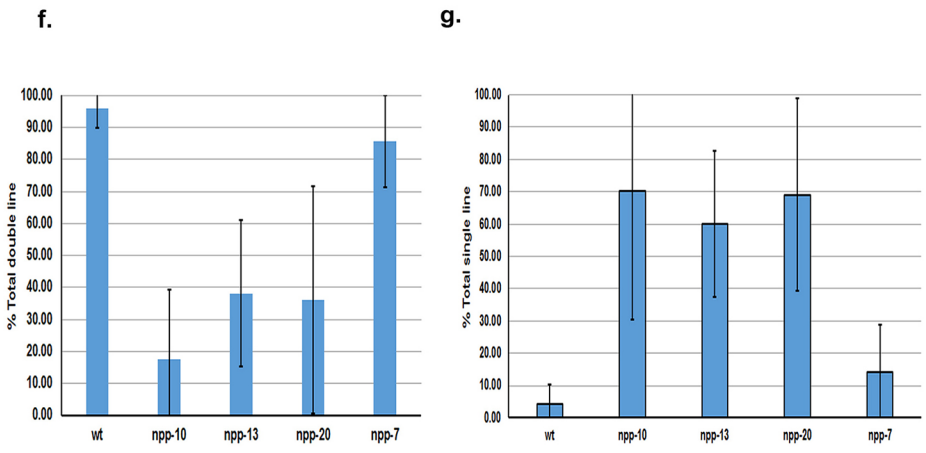

Fig. 4. NPP-10-, NPP-13- and NPP-20 are required for correct centromere assembly and centromere resolution at prometaphase. (A-E) Fixed GFP–HCP-3 transgenic two-cell embryos, treated by RNAi or untreated controls (wild type, WT), were stained with GFP-specific antibodies (red) using indirect immunofluorescence. DNA was counterstained with DAPI (blue). Single channels for DAPI and GFP–HCP-3 are shown in gray scale. Merge: GFP–HCP-3, red; DAPI, blue. Data are displayed as a projection of stacks of deconvolved images. Rightmost column represents a zoomed part of the corresponding merged image. (A) Untreated WT control; (B) *npp-10* RNAi; (C) *npp-13* RNAi; (D) *npp20* RNAi; (E) *npp-7* RNAi. Scale bars: 4 µm. (F) Quantification of prometaphase chromosomes showing centromere resolution (double line) for untreated controls and RNAi-treated animals, indicated as a percent of all chromosomes inspected. (G) Quantification of prometaphase chromosomes failing to resolve centromeres (single line) for untreated controls and RNAi-treated animals indicated as a percent of all chromosomes inspected. For numerical data for F and G, see Table S1A. For details of the quantification method, see Materials and Methods. Data are mean±s.d.

The same was observed following knockdown of NPP-13 and NPP-20 (Fig. S3L,M). Here too, HCP-4 was clearly present close to or in between the condensing prometaphase chromosomes but did not incorporate into the centromeres. Following *npp-7* RNAi, we did not observe this phenotype, and HCP-4 was incorporated into centromeres in a similar manner to that seen in wild type (Fig. 6C). Still later, at metaphase of *npp-10* RNAi-treated embryos, HCP-4 had still not been incorporated into centromeres (Fig. 6E). We conclude that beyond a critical time span, HCP-4 is unable to assemble into centromeres.

Journal of Cell Science (2017) 130, 963-974 doi:10.1242/jcs.196709

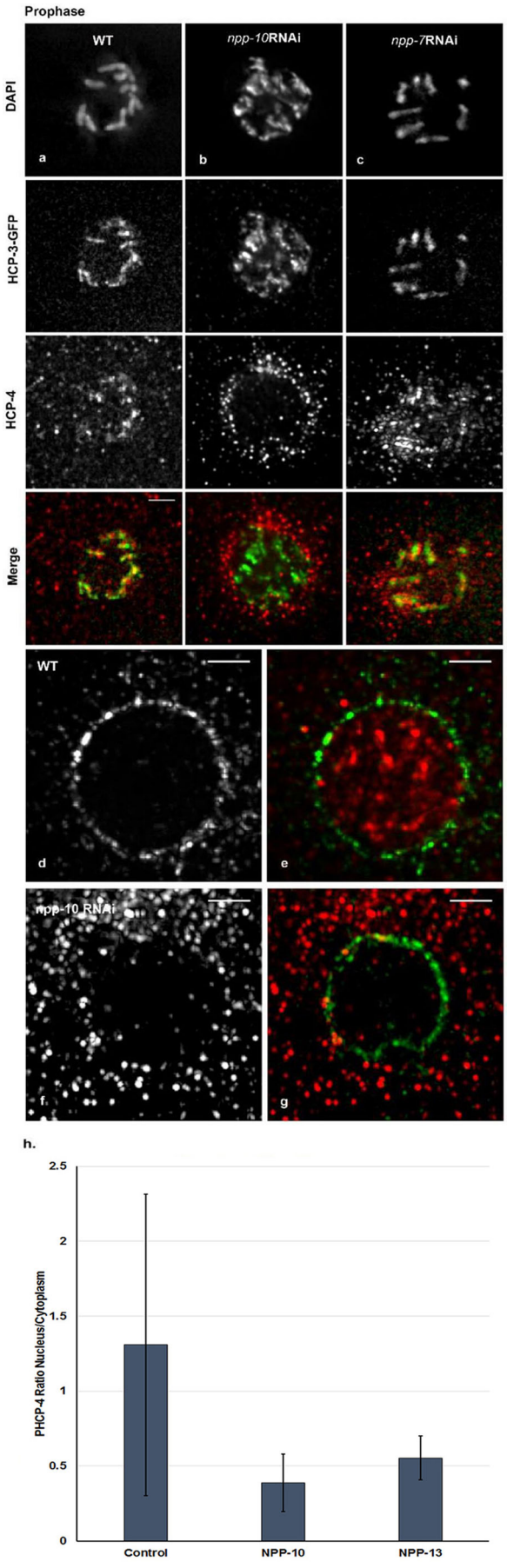

Fig. 5. Knockdown of NPP-10 results in nuclear exclusion of HCP-4 at prophase. Fixed GFP–HCP-3 transgenic two-cell embryos, treated by RNAi or untreated controls (wild type, WT), were stained using indirect immunofluorescence. Data are displayed as a projection of stacks of deconvolved images. (A-C) Nuclei were stained with GFP-specific antibodies (green channel) and antisera against HCP-4 (red channel); DAPI, blue. Single channels for DAPI, GFP–HCP-3 and HCP-4 are shown in gray scale. Merged images: GFP–HCP-3, green; HCP-4, red; (A) untreated WT control; (B) *npp-10* RNAi; (C) *npp-7* RNAi; (D-G) antiserum against HCP-4 (red) and lamin-specific antibodies (green); (D,E) untreated WT control; (D) Lamin channel (gray scale); (E) merge, HCP-4 (red), lamin (green); (F,G) *npp-10* RNAi; (F) HCP-4 channel (gray scale); (G) merge, HCP-4 (red), lamin (green). Scale bars: 4 µm. (H) Nuclear-to-cytoplasmic ratio of HCP-4 in prophase cells (n=5 for each condition; normalized to corresponding cytoplasmic staining taken as 1) for wild-type or NPP-10 and NPP-10 knockdown animals; for individual data points, see Table S2; for more details refer to Materials and Methods. Data are mean±s.d.

DISCUSSION

We found that a subset of nucleoporins is required for correct centromere resolution during prophase. Our data suggest that these proteins play a role in the import of HCP-4 and mediate the timing of HCP-4 availability in the nucleus (Fig. 7). Normally, the bulk of HCP-4 is excluded from nucleus during interphase (Fig. 7A). It enters the nuclear compartment during prophase and is recruited to the maturing centromere through interaction with HCP-3 (Fig. 7B) and KNL-2. In prophase it facilitates the correct centromere resolution on the opposite faces of the sister chromatids (Fig. 7C). If nuclear import of HCP-4 is blocked, an immature centromere forms (Fig. 7D), centromere resolution is abrogated and no functional kinetochore is formed (Fig. 7F). The delayed nuclear accessibility of HCP-4 following nuclear envelope breakdown in prometaphase is insufficient to restore HCP-4 incorporation into centromeres and fails to rescue centromere resolution. This suggests that the timing of the HCP-4 availability at the centromere is critical. Our observations raise a number of questions: how is the import and chromosomal binding of HCP-4 regulated? What is the role of the nucleoporins involved? Finally, why is the timing of nuclear availability critical for HCP-4 incorporation and what is the early role of HCP-4 in centromere formation and resolution?

During interphase, HCP-4 is primarily distributed in the cytoplasm (Moore and Roth, 2001), with a smaller fraction also present in the nucleus. The nuclear-to-cytoplasmic ratio quite dramatically changes at prophase when HCP-4 accumulates in the nucleus and is targeted to centromeres by HCP-3 (Fig. 5). Although the signals that trigger this change in distribution are unknown, protein phosphorylation would be an attractive mechanism since it allows a precise coordination with the cell cycle by cyclin-regulated kinases and phosphatases. In humans, Aurora B kinase promotes KMN network recruitment to HCP-4/CENP-C (Rago et al., 2015), and in *Xenopus*, CENP-C is an integral component for the establishment of kinetochores, the assembly of which depends on several kinases but is suppressed by protein phosphatase 1 (Wynne and Funabiki, 2015). Control of stability of the HCP-4/CENP-C homolog by phosphorylation has been observed in yeast (Peng et al., 2011), and in *Drosophila*, the interaction of CENP-C with protein phosphatase 4 (PP4) is required to maintain CENP-C and attached kinetochore proteins at the chromosomes (Lipinszki et al., 2015). Furthermore, a contribution of sumoylation to CENP-C function has been suggested (Meluh and Koshland, 1995; Fukagawa et al., 2001; Chung et al., 2004).

Whatever the triggering mechanism, our data suggest an active transport of HCP-4 towards the nuclear periphery that is correlated with, but not dependent on, nuclear import. Following knockdown of the nucleoporin genes *npp-10*, *npp -13* and *npp-20*, we observed

Journal of Cell Science (2017) 130, 963-974 doi:10.1242/jcs.196709

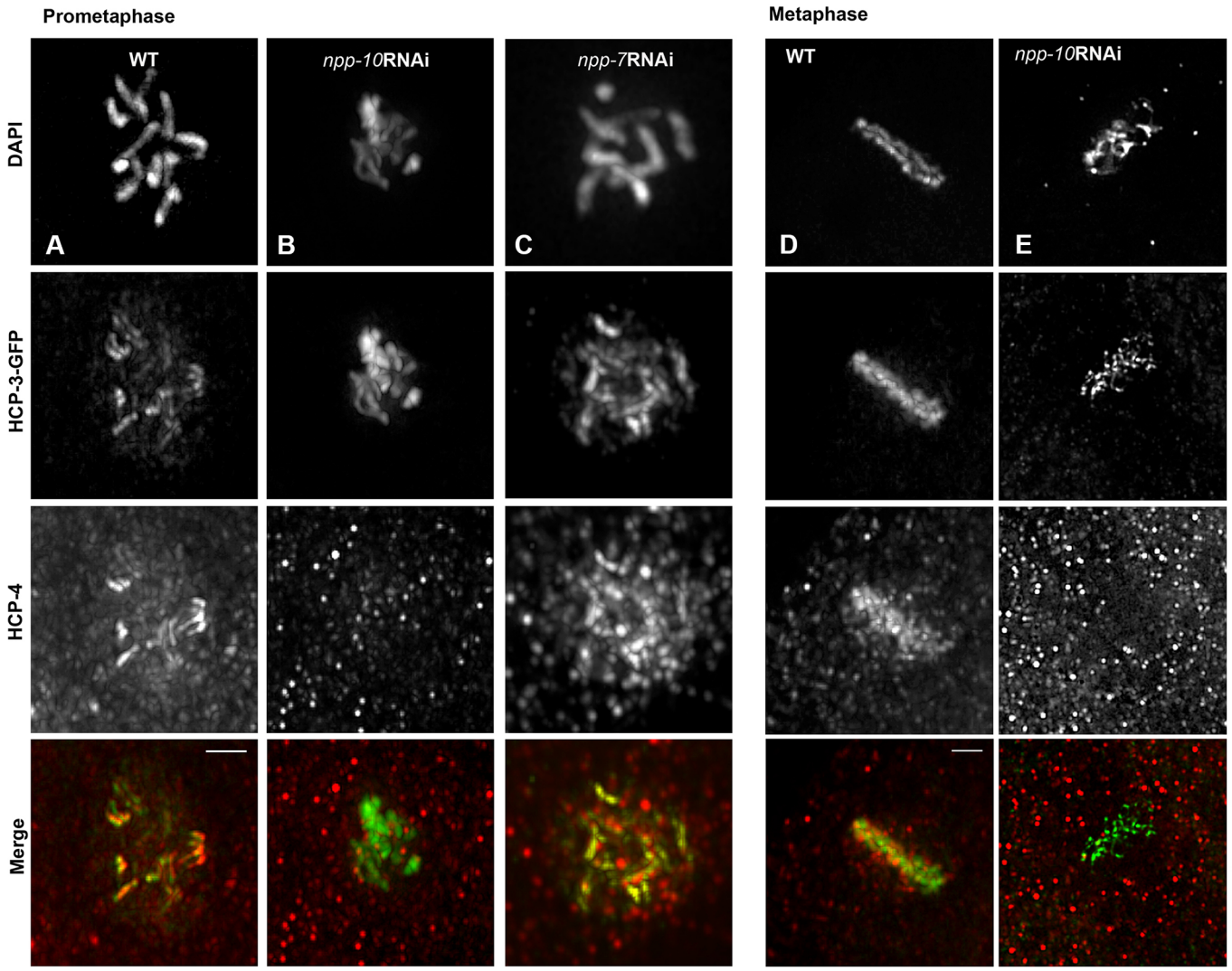

Fig. 6. Following knockdown of NPP-10, HCP-4 is not assembled in centromeres, even after nuclear envelope breakdown. Fixed GFP–HCP-3 transgenic two-cell embryos, treated by RNAi or untreated controls (wild type, WT), were stained using indirect immunofluorescence. Data are displayed as a projection of stacks of deconvolved images. Nuclei were stained with GFP-specific antibodies (green), antisera against HCP-4 (red), DAPI (blue). Single channels for DAPI, GFP–HCP-3 and HCP-4 staining are shown in gray scale. Merged images: GFP–HCP-3 (green) and HCP-4 (red). (A-C) Prometaphase: (A) untreated WT control; (B) *npp-10* RNAi; (C) *npp-7* RNAi. (D-E) Metaphase: (D) untreated WT control; (E) *npp-10* RNAi. Scale bars: 4 µm.

a significant perinuclear enrichment of HCP-4 during prophase (Fig. 5; Fig. S3). This supports the argument for an active cytoplasmic transport of HCP-4, which is triggered in prophase but is stalled at the nuclear envelope due to damaged pore function. In contrast, normally, the import of HCP-4 via the nuclear pores coordinately increases at that time. The mechanism regulating the timed nuclear import of HCP-4 is still unclear. However, the observation that only three of six tested essential nucleoporin genes show a defect in HCP-4 import argues for a specific role for these three genes. In the following discussion, we will concentrate on the proteins encoded by *npp-10*, *npp-13* and *npp-20* and their possible functions in HCP-4 transport.

NPCs comprise multiple copies of about 30 different nucleoporins (Rout et al., 2000; Cronshaw et al., 2002; review by Raices and D′Angelo, 2012). Biochemical and genetic evidence indicates that several nucleoporins are organized in discrete evolutionarily conserved subcomplexes with specific functions (Grandi et al., 1997; Siniossoglou et al., 2000; Belgareh et al., 2001; Theerthagiri et al., 2010; Ródenas et al., 2012). The *C. elegans* NPP-13 is homologous to the yeast Nic96p and human Nup93 protein (Grandi et al., 1997). Nup93 localizes at the nuclear basket or near to the nuclear entry of the gated pore. It is a central component of the Nup93 subcomplex, comprised of five proteins, which is important for NPC assembly and distribution in the nuclear envelope (Grandi et al., 1997; Galy et al., 2003). In *C. elegans*, knockdown of NPP-13 increases the nuclear pore permeability from 45 kD to approximately 70 kD and induces abnormal chromatin condensation (Galy et al., 2003). Even the increased permeability resulting from knockdown would still require active import of the 186 kD HCP-4 protein via the NPC, which for unknown reasons is severely limited by the lack of NPP-13.

The *C. elegans* nucleoporins NPP-10C (*Saccharomyces cerevisiae* Nup145 C-terminal domain and human Nup96) and NPP-20 (*S. cerevisiae* Sec13 and human SEC13) are conserved in the yeast Nup84 subcomplex (Siniossoglou et al., 1996, 2000; Belgareh et al., 2001), and in the corresponding vertebrate Nup107 complex. The Nup107 subcomplex is composed of nine different nucleoporins, including the NPP-10C and NPP-20 homologs. It

Journal of Cell Science (2017) 130, 963-974 doi:10.1242/jcs.196709

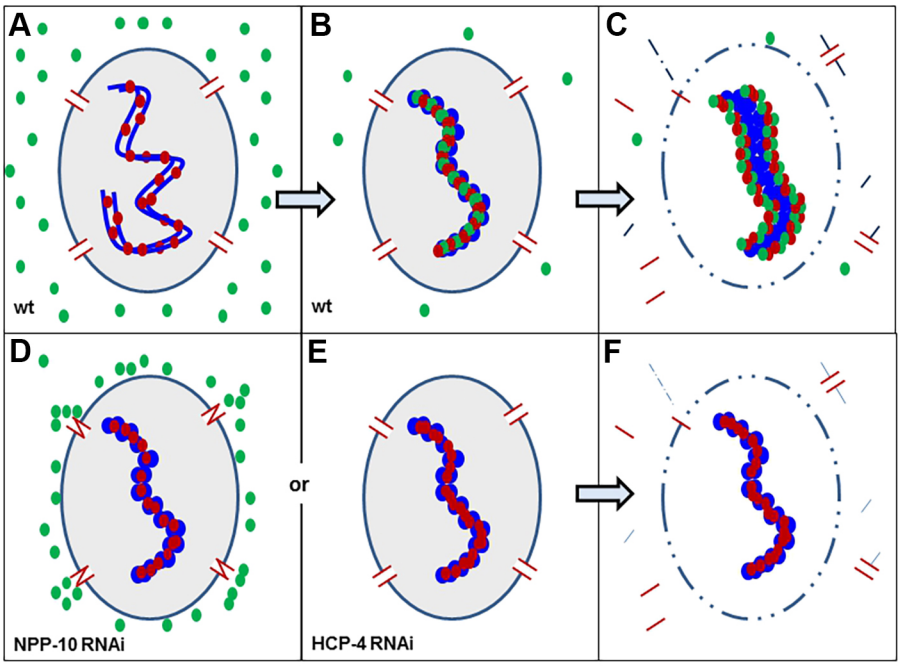

Fig. 7. Model to explain the requirement of nucleoporins for correct centromere assembly in *C. elegans*. (A) A wild-type (wt) nucleus with chromatin (blue) in interphase (G2): the dispersed centromeric units bind to HCP-3 (red); HCP-4 (green) is still in the cytoplasm. (B) A wt nucleus in prophase: a centromere bound to HCP-3 (red) targets imported HCP-4 (green) to immature single-line centromeres. (C) A wt nucleus in late prophase: the mature double-line centromere resolves to the opposite faces of the mitotic chromosome and later forms functional kinetochores. (D) Following RNAi knockdown of *npp-10* (same applies to *npp-13* and *npp-20*), HCP-4 (red) fails to enter the nucleus in prophase. (F) Consequently, HCP-3 on condensing chromosomes forms immature centromeres, which fail to resolve, resulting in defective kinetochores. (E) Similarly, following knockdown of HCP-4, HCP-3 (red) on condensing chromosomes forms immature centromeres, (F) which later result in defective kinetochores (Moore and Roth, 2001). Nucleoplasm in gated nuclei, gray.

forms a part of the NPC scaffold and is critical for NPC reassembly during mitosis. (Belgareh et al., 2001; Walther et al., 2003; Loïodice et al., 2004; Brohawn and Schwartz, 2009). NPP-10C/Nup96 is produced by conserved proteolytic processing of a Nup98-Nup96 precursor protein into the Nup98/NPP-10N and Nup96/NPP-10C nucleoporins (Teixeira et al., 1997; Fontoura et al., 1999). Since both proteins are encoded by the same target mRNA, both are simultaneously affected in *npp-10* RNAi embryos. NPP-20/Sec13 was originally identified as a subunit of the COPII complex involved in vesicle transport (Barlowe et al., 1994). Purified *S. cerevisiae* Nup84 complexes revealed a Y-shaped structure (Siniossoglou et al., 2000) with *S. cerevisiae* Nup145C (NPP-10C) and *S. cerevisiae* Sec13 (NPP-20) in the stalk region of the Y structure (Lutzmann et al., 2002). The crystal structure of the Nup84–Nup145C–Sec13 unit of the Y-complex revealed similarities to the Sec31 edge element in the COPII vesicle lattice. This is consistent with a role of this heterotrimeric unit as an element of a lattice stabilizing the membrane curvature at the nuclear envelope (Brohawn and Schwartz, 2009). Interestingly, both NPP-10C and NPP-20 belong to this unit and might affect transport of HCP-4 through a related mechanism that is yet to be discovered.

Nup98, the homolog of NPP-10N, is the N-terminal product of proteolytic processing of the Nup98-Nup96 precursor (Teixeira et al., 1997; Fontoura et al., 1999). Nup98/NPP-10C is an FG-protein with GFLG repeats, which contribute to nuclear trafficking (reviewed by Iwamoto et al., 2010). It is important for RNA export (Powers et al., 1997), however, its participation in protein import is disputed (Powers et al., 1997; Wu et al., 2001). Experiments with cells expressing mutated Nup98 have indicated a selective requirement in protein import (Wu et al., 2001; Iwamoto et al., 2010). Nup98 localizes on both sides of the NPC (Iwamoto et al., 2010). On the cytoplasmic side, it interacts directly with Nup188 and on the nuclear side it directly binds to Nup96, indicating a polarized orientation that may be functional for directed transport (Griffis et al., 2003). However, more recently, this view was challenged by data placing Nup98 at the center of the NPC, where it interacts with Nup96/NPP-10C in the Nup107 complex (Chatel et al., 2012). This supports the argument that NPP-10C, NPP-10N and NPP-20 are mediators of a common pore function that is required for HCP-4 import. Interestingly, Laurell and coworkers (2011) have reported that hyperphosphorylation of Nup98 drives NPC disassembly and increases nuclear envelope permeability at the onset of mitosis. The release of Nup98 appears to be rate limiting in these processes since mutation of the phosphorylation sites results in a ~20 min delay in NPC breakdown and concomitant delay of increase in permeability in early prophase (Laurell et al., 2011). Therefore, in addition to restricting NPC import, NPP-10N/Nup98 knockdown may affect nuclear availability of HCP-4 through a delay in the increase in nuclear envelope permeability at early prophase. Altered binding of NPP-10N/Nup98 at the pore caused by knockdown of NPP-10C/Nup96 or NPP-20/Sec13 might have similar effects. To sum up, the spatial arrangement of NPP-10C, NPP-10N and NPP-20 in the NPC is consistent with a common still unknown mechanism that is required for HCP-4 nuclear import.

Why is timing of the nuclear import critical for HCP-4 assembly in the centromere? There are two possible scenarios. Binding of HCP-4 may require a more open state of centromeric chromatin, which is still present early in prophase. In the absence of HCP-4, excessive interaction of HCP-3 and KNL-2 might result in alterations of centromeric chromatin, which eventually mask available HCP-4-binding sites. This is consistent with the subtle effects on mitotic chromosome condensation, which are observed in the absence of HCP-4 (Maddox et al., 2007). Therefore, HCP-4 entering the nucleus with a delay upon knockdown of NPPs will fail to integrate into the centromere. Alternatively, an activated form of free HCP-4 may be required for centromere binding, which is available for a critical time period only, since it is rapidly inactivated and excluded from centromere binding. Since phosphorylation changes could provide such a mechanism, it would be interesting to study if the state of HCP-4 phosphorylation is altered during mitosis and if it affects HCP-4 incorporation into centromeres. Once bound, HCP-4 has an important early function in centromere resolution, which takes place before spindle attachment (Moore and Roth, 2001; Oegema et al., 2001). Although the details are still unclear, this early function requires removal of chromosome cohesion. Moore and co-workers (2005) have shown that HCP-4 promotes resolution of cohesion

Journal of Cell Science (2017) 130, 963-974 doi:10.1242/jcs.196709

between the sister centromeres by affecting cohesin-dependent processes. They also showed that the condensin II protein HCP-6 is required for centromere resolution through a cohesin-independent process. It might be crucial for the recruitment of topoisomerase II to remove topological links between DNA strands of sister chromosomes, as has been suggested by Stanvitch and Moore (2008). HCP-4 promotes this process by mediating centromere localization of the condensin II subunit HCP-6 (Moore et al., 2005).

In summary, our data demonstrate that the timed nuclear import of HCP-4 at early stages of mitosis is important for the stepwise assembly of a functional centromere in *C. elegans*. This process starts with the transport of HCP-4 to the nuclear periphery, and HCP-4 stops there if nuclear pore function is blocked. The signal that induces the perinuclear recruitment and import of HCP-4 still has to be clarified. Furthermore, we demonstrate that the nucleoporins NPP-10N, NPP-10C, NPP-13 and NPP-20 are essential for mediating the nuclear import of HCP-4. Timed import is essential for HCP-4 recruitment to the centromere and correct sister chromatid resolution. Nuclear accessibility of HCP-4 following nuclear envelope breakdown in prometaphase is not sufficient for HCP-4 centromere binding and function. Although it is still unclear how the permeability to HCP-4 is regulated at prophase, our data suggest that the dynamic regulation of HCP-4 transport and assembly is essential for centromere function.

MATERIALS AND METHODS

C. elegans strains

All strains were grown and maintained on nematode growth medium (NGM) agar plates (NGM; 2.5 g peptone, 3 g NaCl, 17 g agar, to 975 ml H_2O; Byerly et al., 1976). Plates of 35-100 mm in diameter were seeded with 0.05-0.1 ml of *Escherichia coli* OP50 liquid culture (Stiernagle, 2006). The following strains were obtained from the Genetics Center University of Minnesota: wild-type Bristol strain N2; OD139 strain *ltIs37* [*pAA64; pie-1::mCherry::HIS-58;unc-119(+)*] *qaIs3502*[*unc-119(+); pie-1::YFP::LMN-1*] (Portier et al., 2007; this strain expresses mCherry-labeled histone H2A and YFP-labeled Lamin 1 in early embryos); OD31 strain *ltIs22*[*pPM3; pie-1::GFP-TEV-STag::KNL-2+unc-119(+)*] (Maddox et al., 2007; this strain expresses GFP-labeled KNL-2 in early embryos). Strains were maintained under standard conditions, between 15°C and 20°C (Brenner, 1974; Stiernagle, 2006). To obtain a strain expressing HCP-3 fused to the GFP reporter, *hcp-3* genomic DNA and cDNA were cloned into the pAZ-LAP(N)-GFP vector (Praitis et al., 2001) using the SpeI restriction site. By using the *pie-1* promoter and enhancer system (Strome et al., 2001), these proteins were exclusively expressed in the germline and in early one- to two-cell embryos. The plasmid was introduced into the *unc-119 (ed3)* strain, using the high-pressure microparticle bombardment method developed by Praitis et al., 2001. For ballistic bombardment, we used PDS-1000/He (Bio-Rad) from MPI-CBG (Dr Anthony Hyman, Dresden). Pressurized helium was used to 'bombard' small transgene-coated gold particles at high speeds into the worm tissue (Jackstadt et al., 1999; Praitis, 2006; Isik and Berezikov, 2013). Bombardments were performed with the DP38 strain worms harboring the *unc-119 (ed3)* mutation. Transgenic animals showing coordinated movement were selected from surviving dauer, stage progeny. Untransformed worms on the same plate remained uncoordinated and died.

RNAi

We generated templates for the production of dsRNAs, as described by Moore et al. (1999). Sequences representing a portion of exons of each gene were amplified from wild-type genomic DNA of Bristol strain N2 using primers for the sense strand with or without T7 promoter sequences (5′-TAATACGACTCACTATAGGGA-3′) at their 5′-end, and primers for the antisense strand with or without T7 promoter sequences at their 5′-end. dsRNA was synthesized using T7 RNA polymerase and diluted in water to a final concentration of 5 µg/µl. The primers used were obtained by Invitrogen Life Technologies and are as follows. Note, that the 5′ T7 promoter sequences attached to some of the oligonucleotides were not included: amplicon *hcp-3* (654 bp): sense *hcp-3*: 5′-GTCGGCAGAAATTC-3′, antisense *hcp-3* 5′-GAATCAGAAGGTCTTCAG-3′; amplicon hcp-4 (982 bp): sense *hcp-4*: 5′-CTGTTCACACCAAGTCTG-3′, antisense *hcp-4*: 5′-GGAGTTGCGGCTTTCGA-3′; amplicon npp-7 (908 bp): sense *npp-7*: 5′-CACGTGTTGATTGGGAGTG-3′, antisense *npp-7*: 5′-GTCGAATCAGCAGGCTTTG-3′; amplicon npp-8 (542 bp): sense *npp-8*: 5′-CCTGCCGATTCAGCTACC-3′, antisense *npp-8*: 5′-GTCGAATCAG-CAGGCTTTG-3′; amplicon npp-10 (1396 bp): sense *npp-10*: 5′-GCGA-CAAATGCTTTCGG-3′, antisense *npp-10*: 5′-CAACAATCTCGTCGA-GAGC-3′; amplicon npp-13 (395 bp): sense *npp-13*: 5′-CCAACCAGAA-GACGACAG, antisense *npp-13*: 5′-CAGAAACCGCTTTCTGAACC-3′; amplicon npp-20 (258 bp): sense *npp-20*: 5′-GGAACGAACAACAAGG-CCG-3′, antisense *npp-20*: 5′-GACGTTTTTTTGCCGCCG-3′.

For RNAi experiments using the soaking method (Tabara et al., 1998), synchronous worm populations from hatching L larvae were grown until they reached the L4/young adult stage. Worms were added to 10 µl drops of dsRNA (5 µg/µl) containing 5 mM spermidine on a piece of parafilm and soaked at 20°C overnight in a humid chamber. Then, worms were transferred to fresh plates and allowed to recover for 12–24 h. Starting from 8 h, incubated worm embryos were examined for RNAi-induced phenotypes. To determine embryonic lethality, 4-6 worms were moved to an individual NGM plate and allowed to lay eggs overnight. Adult worms were removed from the plates, and unhatched embryos were counted on the plates the next day.

Immunostaining and microscopy

Worms were chopped, placed on a Superfrost Ultra Plus slide (Carl Roth, Germany) and either frozen in liquid nitrogen for long-term storage or directly fixed in cold MeOH. Subsequently, blocking solution (3% BSA in PBS) was added. Incubation with primary antibodies was for 2 h at room temperature. As primary antibodies, we used rabbit anti-HCP-3 (Buchwitz et al., 1999; 1:200), rabbit anti-HCP-4 (Moore and Roth, 2001; 1:200), rabbit anti-NPP-10N (provided by Dr Iain Mattaj, EMBL, Heidelberg, Germany; and Dr Matyas Gorjanacz, Bayer Pharma AG, Leverkusen, Germany; 1:500), rabbit anti-NPP-13 (from Dr Iain Mattaj; 1:500) and rabbit anti-NPP-7 (provided by Dr Claudio Aséncio; 1:500) antibodies. Nuclear pores were visualized using the monoclonal antibody MAb 414 from Abcam (ab24609; 1:5000), nuclear lamina was stained using anti-lamin-I antibodies from Abmart [X1-Q21443 (ABX; 1:300)], GFP antibodies were from Abcam (Ab6556; 1:300). After washing twice, secondary antibodies were applied. As secondary antibodies, we used: Alexa-Fluor-488- and Alexa-Fluor-555-conjugated goat anti-mouse-IgG or goat anti-rabbit-IgG antibodies (Life Technologies). Slides were washed twice, with DAPI (1 mg/ml) added to the second wash in a 1:25,000 fold dilution. Slides were mounted in 85% glycerol, 3% (w/v) n-propyl-gallate and directly inspected by microscopy or stored frozen at −20°C.

Live and fixed samples were imaged using an Olympus IX70 Deltavision microscope (Applied Precision) with a 100×/1.40 Plan Apo or a 60×/1.40 Plan Apo oil immersion objective. Images were collected with a Photometrics CH350 digital camera. All images were collected at the indicated wavelengths as stacks of 0.2-µm optical sections. The image stacks were subsequently deconvolved, using the softWoRx software (Applied Precision) and examined as either single sections or as projections of the entire stack (Hiraoka et al., 1991; Meister et al., 2010). Images were further analyzed and processed using a quantitative image analysis tool, ImageJ (National Institutes of Health), and Photoshop® CS2 (Acrobat Adobe). For real-time imaging, embryos were placed on an agarose pad (1% agarose in M9 buffer: 22 mM KH_2PO_4, 43 mM K_2HPO_4, 86 mM NaCl, 1 mM $MgSO_4$, in 800 ml of H_2O), and examined using the Deltavision microscope as described. One-cell embryos were examined until they began to undergo their first cleavage division, generating the AB and P1 blastomeres. Immediately following this division, the progression of the AB nucleus through the cell cycle was recorded at 22°C, with time points collected every 30 s. For every time point, 20×0.2 µm optical sections were taken. In most cases, a complete mitotic cycle could be observed. For time-lapse images of embryos, mitotic stages were determined using the time that had elapsed. For

fixed samples, the presence/absence of nuclear envelope staining by Mab 414 was used to distinguish between prophase and prometaphase embryos.

Quantification of the rate of sister centromere resolution

GFP–HCP-3 or GFP–KNL-2 transgenic embryos, treated using RNAi or untreated controls (wild type), were stained with anti-GFP-antibodies and with MAb414. For each condition, 19 two-cell embryos with cytologically distinct prometaphase chromosomes, lacking a nuclear envelope as evident by Mab414 staining (see Materials and Methods), were randomly chosen for evaluation. Distinct chromosomes with a double-line pattern indicating centromere resolution were counted as 'double line' chromosomes. Distinct chromosomes with a single-line pattern indicating non-resolved centromeres were counted as 'single line' chromosomes. For each condition, the mean and standard deviation of all double-line or single-line chromosomes were determined and expressed as a percentage of all chromosomes analyzed (Table S1).

Quantification of the nuclear-to-cytoplasmic ratio of HCP-4 staining in prophase embryos

To determine the ratio of HCP-4 in the nuclear versus the cytoplasmic compartment of wild-type and RNAi-knockdown animals, embryos were double-stained for HCP-4 and the nuclear pore complex (MAb 414), and recorded as stacks of 22 images. Five randomly chosen prophase cells were evaluated for each condition. For each section of the stacks, the mean intensity of HCP-4 staining in the nuclear (delineated by MAb414) and in an adjacent cytoplasmic region of same size was determined, both corrected for background by subtracting the minimal pixel intensity of the whole stack. Using these data, the mean intensity for the nuclear or cytoplasmic compartment in the whole stack was determined and used to calculate the nuclear-to-cytoplasmic ratio for the given cell. The mean and standard deviation of all five cells of a given condition was calculated and was displayed as the ratio of the nuclear-to-cytoplasmic HCP-4 staining normalized to the cytoplasmic staining (=1) for that condition (Table S2; Fig. 5H). The relative import efficiency as a percentage was calculated from these nuclear-to-cytoplasmic staining ratios normalized to the wild-type staining ratio according to: import efficiency = nuclear-to-cytoplasmic ratio NPP RNAi × 100/nuclear-to-cytoplasmic ratio of wild-type control.

Western blot analysis

Probes obtained from 1 g of embryo lysates were separated by SDS-PAGE and transferred to a nitrocellulose membrane. Membranes were incubated overnight at room temperature with the primary antibody solution (1:500 in PBS, BSA 1%), washed in PBS, 0.1% Triton X-100 and probed with horseradish peroxidase-conjugated goat anti-rabbit IgG (Amersham) (1:2000 for 2 h in PBS, 1% BSA). Proteins were visualized using a chemiluminescence reagent kit (Amersham). Membranes were stripped and reprobed using the same method but using anti-α-tubulin and anti-histone-H2A antibodies as loading controls.

Acknowledgements

We thank Dr Anthony Hyman for his support in the biolistic transformation of *C. elegans*. We are grateful to Dr P. Maddox (University of North Carolina, Department of Biology, Chapel Hill, NC), and Dr A. Desai (University of California, Department of Cellular and Molecular Medicine, San Diego, CA) and Dr L. Moore (Fred Hutchinson Cancer Research Center, Seattle, WA) for providing us with anti-HCP-3 and anti-HCP-4 antibodies, respectively. We also thank Dr I. Mattaj (EMBL, Heidelberg, Germany), Dr M. Gorjanacz (Bayer-Healthcare, Leverkusen, Germany), Dr Geraldine Seydoux (Howard Hughes Medical Institute, Johns Hopkins University School Medicine, Baltimore, MD) and Dr C. Aséncio (Pablo Olavide University, Seville, Spain) for providing anti-NPP-10, anti-NPP-13 and anti-NPP-7 anti-rabbit antibodies. We thank Dr Mihaela Anitei for critical reading of the manuscript. The support provided by all members of the Cytogenetics group is also gratefully acknowledged. We are thankful to the *Caenorhabditis* Genetics Center (Department of Genetics, Cell Biology and Development, University of Minnesota, Minneapolis, MN), which is funded by the NIH Office of Research Infrastructure Programs (P40 OD010440), for support and for providing us with some strains.

Competing interests

The authors declare no competing or financial interests.

Author contributions

Experimental work was performed by J.F.; H.S. and J.H.S. were supervisors of the project and contributed to data analysis and writing the manuscript.

Funding

J.H.S. and J.F. were supported by a Deutsche Forschungsgemeinschaft grant (STE 1887/1-1), and the Institute of Biology, Humboldt University, Berlin, Germany.

Supplementary information

Supplementary information available online at
http://jcs.biologists.org/lookup/doi/10.1242/jcs.196709.supplemental

References

Barlowe, C., Orci, L., Yeung, T., Hosobuchi, M., Hamamoto, S., Salama, N., Rexach, M. F., Ravazzola, M., Amherd, M. and Schekman, R. (1994). COPII: A membrane coat formed by Sec proteins which drive vesicle budding from the endoplasmic reticulum. *Cell* **77**, 895-907.

Belgareh, N., Rabut, G., Bai, S. W., van Overbeek, M., Beaudouin, J., Daigle, N., Zatsepina, O. V., Pasteau, F., Labas, V., Fromont-Racine, M. et al. (2001). An evolutionarily conserved NPC subcomplex, which redistributes in part to kinetochores in mammalian cells. *J. Cell Biol.* **154**, 1147-1160.

Brenner, S. (1974). The genetics of *Caenorhabditis elegans*. *Genetics* **77**, 71-94.

Brohawn, S. G. and Schwartz, T. U. (2009). Molecular architecture of the Nup84-Nup145C-Sec13 edge element in the nuclear pore complex lattice. *Nat. Struct. Mol. Biol.* **16**, 1173-1177.

Buchwitz, B. J., Ahmad, K., Moore, L. L., Rotha, M. B. and Henikoff, S. (1999). A histone-H3-like protein in *C. elegans*. *Nature* **401**, 547-548.

Byerly, L., Cassada, R. C. and Russell, R. L. (1976). The life cycle of the nematode *Caenorhabditis elegans*. I. Wild-type growth and reproduction. *Dev. Biol.* **51**, 23-33.

Chatel, G., Desai, S. H., Mattheyses, A. L., Powers, M. A. and Fahrenkrog, B. (2012). Domain topology of nucleoporin Nup98 within the nuclear pore complex. *J. Struct. Biol.* **177**, 81-89.

Cheeseman, I. M. (2014). The kinetochore. *Cold Spring Harb. Perspect. Biol.* **6**, a015826.

Chung, T.-L., Hsiao, H.-H., Yeh, Y.-Y., Shia, H.-L., Chen, Y.-L., Liang, P.-H., Wang, A. H.-J., Khoo, K.-H. and Li, S. S.-L. (2004). In vitro modification of human centromere protein CENP-C fragments by small ubiquitin-like modifier (SUMO) protein. *J. Biol. Chem.* **279**, 39653-39662.

Cronshaw, J. M., Krutchinsky, A. N., Zhang, W., Chait, B. T. and Matunis, M. M. (2002). Proteomic analysis of the mammalian nuclear pore complex. *J.Cell Biol.* **158**, 915-927.

De Rop, V., Padeganeh, A. and Maddox, P. (2012). CENP-A: the key player behind centromere identity, propagation, and kinetochore assembly. *Chromosoma* **121**, 527-538.

Desai, A., Rybina, S., Müller-Reichert, T., Shevchenko, A., Shevchenko, A., Hyman, A. and Oegema, K. (2003). KNL-1 directs assembly of the microtubule-binding interface of the kinetochore in *C.elegans*. *Genes Dev.* **17**, 2421-2435.

Foltz, D. R., Jansen, L. E. T., Bailey, A. O., Yates, J. R., III, Bassett, E. A., Wood, S., Black, B. E. and Cleveland, D. W. (2009). Centromere specific assembly of CENP-A nucleosomes is mediated by HJURP. *Cell* **137**, 472-487.

Fontoura, B. M. A., Blobel, G. and Matunis, M. J. (1999). A conserved biogenesis pathway for nucleoporins: proteolytic processing of a 186-kilodalton precursor generates Nup98 and the novel nucleoporin, Nup96. *J. Cell Biol.* **144**, 1097-1121.

Fukagawa, T. and Earnshaw, W. C. (2014). The centromere: chromatin foundation for the kinetochore machinery. *Dev. Cell* **30**, 496-508.

Fukagawa, T., Regnier, V. and Ikemura, T. (2001). Creation and characterization of temperature-sensitive CENP-C mutants in vertebrate cells. *Nucl. Ac. Res.* **29**, 3796-3803.

Galy, V., Mattaj, I. M. and Askjaer, P. (2003). *Caenorhabditis elegans* nucleoporins Nup93 and Nup205 determine the limit of nuclear pore size exclusion in vivo. *Mol. Biol. Cell* **14**, 5104-5115.

Gascoigne, K. E. and Cheeseman, I. M. (2011). Kinetochore assembly: if you built it, they will come. *Curr. Opin. Cell. Biol.* **23**, 102-108.

Gassmann, R., Rechtsteiner, A., Yuen, K. W., Muroyama, A., Egelhofer, T., Gaydos, L., Barron, F., Maddox, P., Essex, A., Monen, J. et al. (2012). An inverse relationship to germline transcription defines centromeric chromatin in *C. elegans*. *Nature* **484**, 534-537.

Grandi, P., Dang, T., Pane, N., Shevchenko, A., Mann, M., Forbes, D. and Hurt, E. (1997). Nup93, a vertebrate homologue of yeast Nic96p, forms a complex with a novel 205-kDa protein and is required for correct nuclear pore assembly. *Mol. Biol. Cell* **8**, 217-238.

Griffis, E. R., Xu, S. and Powers, M. A. (2003). Nup98 localizes to both nuclear and cytoplasmic sides of the nuclear pore and binds to two distinct nucleoporin subcomplexes. *Mol. Biol. Cell* **14**, 600-610.

Hachet, V., Busso, C., Toya, M., Sugimoto, A., Askjaer, P. and Gönczy, P. (2012). The nucleoporin Nup205/NPP-3 is lost near centrosomes at mitotic onset

and can modulate the timing of this process in *Caenorhabditis elegans* embryos. *Mol. Biol. Cell* **23**, 3111-3121.
Hajeri, V. A., Little, B. A., Ladage, M. L. and Padilla, P. A. (2010). NPP-16/Nup50 function and CDK-1 inactivation are associated with anoxia-induced prophase arrest in *Caenorhabditis elegans. Mol.Biol. Cell* **21**, 712-724.
Hiraoka, Y., Swedlow, J. R., Paddy, M. R., Agard, D. A. and Sedat, J. W. (1991). Three-dimensional multiple-wavelength fluorescence microscopy for the structural analysis of biological phenomena. *Sem. Cell Biol.* **2**, 153-165.
Hori, T., Amano, M., Suzuki, A., Backer, C. B., Welburn, J. P., Dong, Y., McEwen, B. F., Shang, W.-H., Suzuki, E., Okawa, K. et al. (2008). CCAN makes multiple contacts with centromeric DNA to provide distinct pathways to the outer kinetochore. *Cell* **135**, 1039-1052.
Hori, T., Shang, W.-H., Takeuchi, K. and Fukagawa, T. (2013). The CCAN recruits CENP-A to the centromere and forms the structural core for kinetochore assembly. *J. Cell Biol.* **200**, 45-60.
Ikegami, K. and Lieb, J. D. (2013). Integral nuclear pore proteins bind to Pol III-transcribed genes and are required for Pol III transcript processing in *C. elegans*. *Mol. Cell* **51**, 840-849.
Isik, M. and Berezikov, E. (2013). Biolistic transformation of *Caenorhabditis elegans*. *Meth. Mol. Biol.* **940**, 77-86.
Iwamoto, M., Asakawa, H., Hiraoka, Y. and Haraguchi, T. (2010). Nucleoporin Nup98: a gatekeeper in the eukaryotic kingdoms. *Genes Cells* **15**, 661-669.
Jackstadt, P., Wilm, T. P., Zahner, H. and Hobom, G. (1999). Transformation of nematodes via ballistic DNA transfer. *Mol. Biochem. Parasitol.* **103**, 261-266.
Kitagawa, R. (2010). Key players in chromosome segregation in *Caenorhabditis elegans*. *Front. Biosci.* **14**, 1529-1557.
Laurell, E., Beck, K., Krupina, K., Theerthagiri, G., Bodenmiller, B., Horvath, P., Aebersold, R., Antonin, W. and Kutay, U. (2011). Phosphorylation of Nup98 by multiple kinases is crucial for NPC disassembly during mitotic entry. *Cell* **144**, 539-550.
Lipinszki, Z., Lefevre, S., Savoian, M. S., Singleton, M. R., Glover, D. M. and Przewloka, M. R. (2015). Centromeric binding and activity of Protein Phosphatase 4. *Nat. Commun.* **6**, 5894.
Loïodice, I., Alves, A., Rabut, G., van Overbeek, M., Ellenberg, J., Sibarita, J.-B. and Doye, V. (2004). The entire Nup107-160 complex, including three new members, is targeted as one entity to kinetochores in mitosis. *Mol. Biol. Cell* **15**, 3333-3344.
Lutzmann, M., Kunze, R., Buerer, A., Aebi, U. and Hurt, E. (2002). Modular self-assembly of a Y-shaped multiprotein complex from seven nucleoporins. *EMBO J.* **21**, 387-397.
Maddox, P. S., Hyndman, F., Monen, J., Oegema, K. and Desai, A. (2007). Functional genomics identifies a Myb domain-containing protein family required for assembly of CENP-A chromatin. *J. Cell Biol.* **176**, 757-763.
McKinley, K. L. and Cheeseman, I. M. (2014). Polo-like-kinase 1 licenses CENP-A deposition at centromeres. *Cell* **158**, 397-411.
Meister, P., Towbin, B. D., Pike, B. L., Ponti, A. and Gasser, S. M. (2010). The spatial dynamics of tissue-specific promoters during *C.* elegans development. *Genes Dev.* **24**, 766-782.
Meluh, P. B. and Koshland, D. (1995). Evidence that the *MIF2* Gene of *Saccharomyces cerevisiae* encodes a centromere protein with homology to the mammalian centromere protein CENP-C. *Mol. Biol. Cell.* **6**, 793-807.
Moore, L. L. and Roth, M. B. (2001). HCP-4, a CENP-C-like protein in *Caenorhabditis elegans*, is required for resolution of sister centromeres. *J. Cell Biol.* **153**, 1199-1207.
Moore, L. L., Morrison, M. and Roth, M. B. (1999). HCP-1, a protein involved in chromosome segregation, is localized to the centromere of mitotic chromosomes in *Caenorhabditis elegans. J. Cell Biol.* **147**, 471-479.
Moore, L. L., Stanvitch, G., Roth, M. B. and Rosen, D. (2005). HCP-4/CENP-C promotes the prophase timing of centromere resolution by enabling the centromere association of HCP-6 in *Caenorhabditis elegans. Mol. Cell. Biol.* **25**, 2583-2592.
Oegema, K., Desai, A., Rybina, S., Kirkham, M. and Hyman, A. A. (2001). Functional analysis of kinetochore assembly in *Caenorhabditis elegans. J. Cell Biol.* **153**, 1209-1225.
Okada, M., Cheeseman, I. M., Hori, T., Okawa, K., McLeod, I. X., Yates, J. R., III, Desai, A. and Fukagawa, T. (2006). The CENP-H-I complex is required for the efficient incorporation of newly synthesized CENP-A into centromeres. *Nat. Cell Biol.* **8**, 446-457.
Peng, Y., Wong, C. C. L., Nakajima, Y., Tyers, R. G., Sarkeshik, A. S., Yates, J., III, Drubin, D. G. and Barnes, G. (2011). Overlapping kinetochore targets of CK2 and Aurora B kinases in mitotic regulation. *Mol. Biol. Cell* **22**, 2680-2689.
Portier, N., Audhya, A., Maddox, P. S., Green, R. A., Dammermann, A., Desai, A. and Oegema, K. (2007). A Microtubule-Independent Role for Centrosomes and Aurora A in Nuclear Envelope Breakdown. *Dev. Cell* **12**, 515-529.
Powers, M. A., Forbes, D. J., Dahlberg, J. E. and Lund, E. (1997). The vertebrate GLFG nucleoporin, Nup98, is an essential component of multiple RNA export pathways. *J. Cell Biol.* **136**, 241-250.
Praitis, V. (2006). Creation of transgenic lines using microparticle bombardment methods. *Meth. Mol. Biol.* **351**, 93-107.
Praitis, V., Casey, E., Collar, D. and Austin, J. (2001). Creation of low-copy integrated transgenic lines in *Caenorhabditis elegans*. *Genetics* **157**, 1217-1226.
Rago, F., Gascoigne, K. E. and Cheeseman, I. M. (2015). Distinct organization and regulation of the outer kinetochore KMN network downstream of CENP-C and CENP-T. *Curr. Biol.* **25**, 671-677.
Raices, M. and D'Angelo, M. A. (2012). Nuclear pore complex composition: a new regulator of tissue-specific and developmental functions. *Nat. Rev. Mol. Biol.* **13**, 687-699.
Ródenas, E., Klerkx, E. P. F., Ayuso, C., Audhya, A. and Askjaer, P. (2009). Early embryonic requirement for nucleoporin Nup35/NPP-19 in nuclear assembly. *Dev. Biol.* **327**, 399-409.
Ródenas, E., Gonzalez-Aguilera, C., Ayuso, C. and Askjaer, P. (2012). Dissection of the Nup107 nuclear pore subcomplex reveals a novel interaction with spindle assembly checkpoint protein MAD1 in *Caenorhabditis elegans*. *Mol. Biol. Cell* **23**, 930-944.
Rout, M. P., Aitchison, J. D., Suprapto, A., Hjertaas, K., Zhao, Y. and Chait, B. T. (2000). The yeast nuclear pore complex: Composition, architecture and transport mechanism. *J. Cell Biol.* **148**, 635-652.
Saitoh, H., Tomkiel, J., Cooke, C. A., Ratrie, H., III, Maurer, M., Rothfield, N. F. and Earnshaw, W. C. (1992). CENP-C, an autoantigen in scleroderma, is a component of the human inner kinetochore plate. *Cell* **70**, 115-125.
Schetter, A., Askjaer, P., Piano, F., Mattaj, I. and Kemphues, K. (2006). Nucleoporins NPP-1, NPP-3, NPP-4, NPP-11 and NPP-13 are required for proper spindle orientation in *C.elegans. Dev. Biol.* **289**, 360-371.
Siniossoglou, S., Wimmer, C., Rieger, M., Doye, V., Tekotte, H., Weise, C., Emid, S., Segref, A. and Hurt, E. C. (1996). A novel complex of nucleoporins, which includes Sec13p and Sec13p homolog, is essential for normal nuclear pores. *Cell* **84**, 265-275.
Siniossoglou, S., Lutzmann, M., Santos-Rosa, H., Leonard, K., Mueller, S., Aebi, U. and Hurt, E. (2000). Structure and assembly of the Nup84p complex. *J. Cell Biol.* **149**, 41-54.
Stanvitch, G. and Moore, L. L. (2008). *cin-4*, a gene with homology to topoisomerase I, is required for centromere resolution by cohesion removal from sister kinetochores during mitosis. *Genetics* **178**, 83-97.
Steiner, F. A. and Henikoff, S. (2014). Holocentromeres are dispersed point centromeres localized at transcription factor hotspots. *ELife* **3**, e02025.
Stiernagle, T. (2006). Maintenance of *C. elegans*. *WormBook* 1-11.
Strome, S., Powers, J., Dunn, M., Reese, K., Malone, C. J., White, J., Seydoux, G. and Saxton, W. (2001). Spindle dynamics and the role of γ-tubulin in early *C. elegans Embryos*. *Mol. Biol. Cell.* **12**, 1751-1764.
Tabara, H., Grishok, A. and Mello, C. C. (1998). RNAi in *C. elegans*: soaking in the genome sequence. *Science* **282**, 430-431.
Takeuchi, K., Nishino, T., Mayanagi, K., Horikoshi, N., Osakabe, A., Tachiwana, H., Hori, T., Kurumizaka, H. and Fukagawa, T. (2014). The centromeric nucleosome-like CENP-T-W-S-X complex induce positive supercoils into DNA. *Nucleic Acids Res.* **42**, 1644-1655.
Teixeira, M. T., Siniossoglou, S., Podtelejnikov, S., Mann, M., Dujon, B., Hurt, E. and Fabre, E. (1997). Two functionally distinct domains generated by in vivo cleavage of Nup145p: a novel biogenesis pathway for nucleoporins. *EMBO J.* **16**, 5086-5097.
Theerthagiri, G., Eisenhardt, N., Schwarz, H. and Antonin, W. (2010). The nucleoporin Nup188 controls passage of membrane proteins across the nuclear pore complex. *J. Cell Biol.* **189**, 1129-1142.
Walther, T. C., Alves, A., Pickersgill, H., Loï¨odice, I., Hetzer, M., Galy, V., Hülsmann, B. B., Köcher, T., Wilm, M., Allen, T. et al. (2003). The conserved Nup107-160 complex is critical for nuclear pore complex assembly. *Cell* **113**, 195-206.
Wan, J., Subramonian, D. and Zhang, X.-D. (2012). SUMOylation in control of accurate chromosome segregation during mitosis. *Curr. Prot. Pept. Sci.* **13**, 467-481.
Wu, X., Kasper, L. H., Mantcheva, R. T., Mantchev, G. T., Springett, M. J. and van Deursen, J. M. A. (2001). Disruption of the FG nucleoporin Nup98 causes selective changes in nuclear pore complex stoichiometry and function. *Proc. Natl. Acad. Sci. USA* **98**, 3191-3196.
Wynne, D. J. and Funabiki, H. (2015). Kinetochore function is controlled by a phospho-dependent coexpansion of inner and outer components. *J. Cell Biol.* **210**, 899-916.
Yamagishi, Y., Sakuno, T., Goto, Y. and Watanabe, Y. (2014). Kinetochore composition and its function: lessons from yeasts. *FEMS Microbiol. Rev.* **38**, 185-200.
Yanagida, M. (2005). Basic mechanism of eukaryotic chromosome segregation. *Phil. Trans. R. Soc. B Biol. Sci.* **360**, 609-621.

Journal of Cell Science

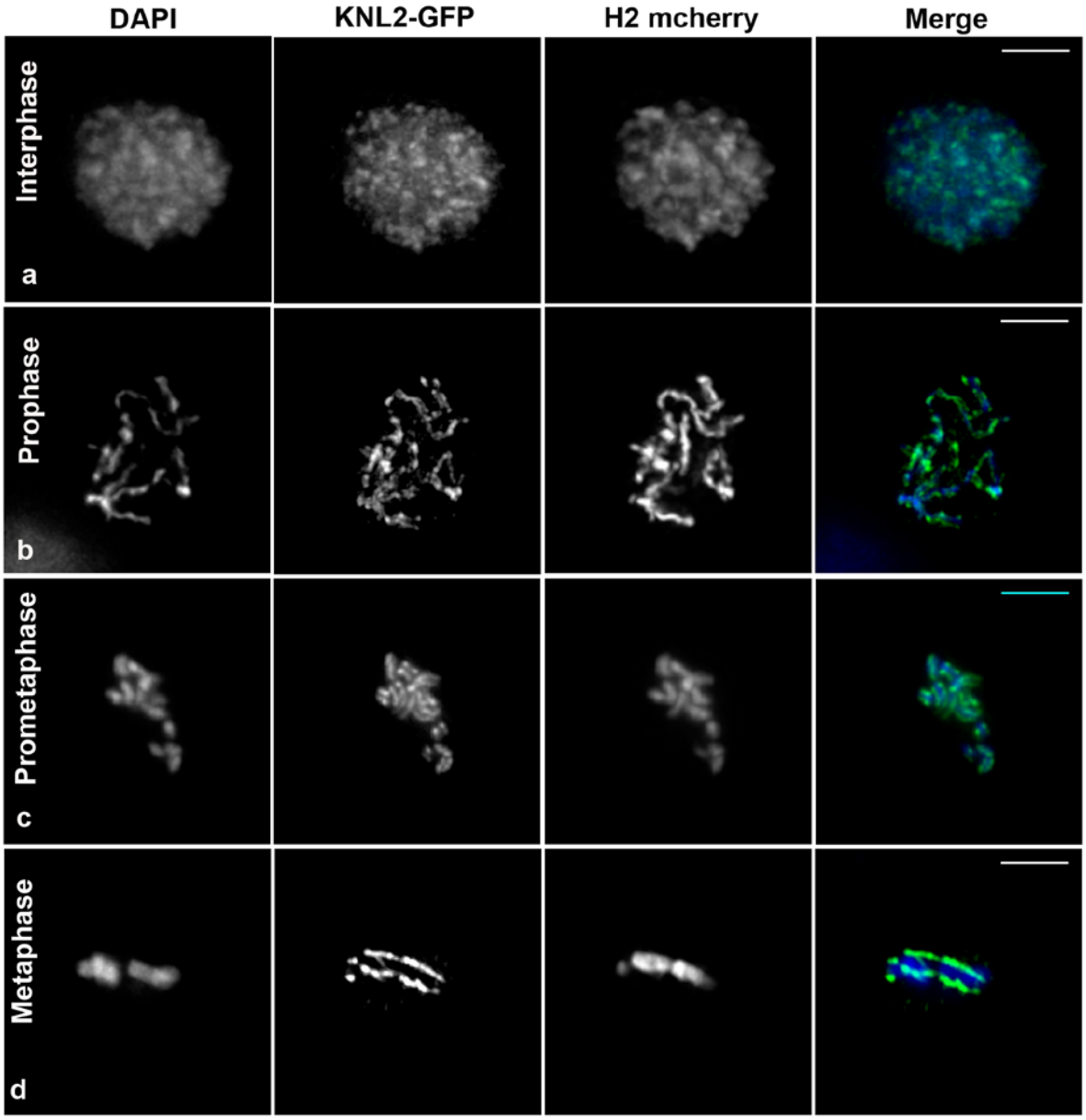

Supplementary material Figure S1: Centromere formation in *C. elegans* 2-cell embryos : Fixed embryos of a strain double transgenic for KNL-2-GFP and histone H2A-cherry were stained with GFP- and mCherry- antibodies by indirect immunofluorescence. DNA was stained by DAPI and data were recorded by image restoration microscopy. Data are displayed as a projection of stacks of deconvolved images. Single channels in grey scale for DAPI, KNL-2 and H2A-cherry as indicated on the top; merge: GFP-KNL-2 green, DAPI blue. From top to bottom a) interphase ; b) prophase ; c) prometaphase d ; metaphase. Bar 4 μm.Compare movie 1.

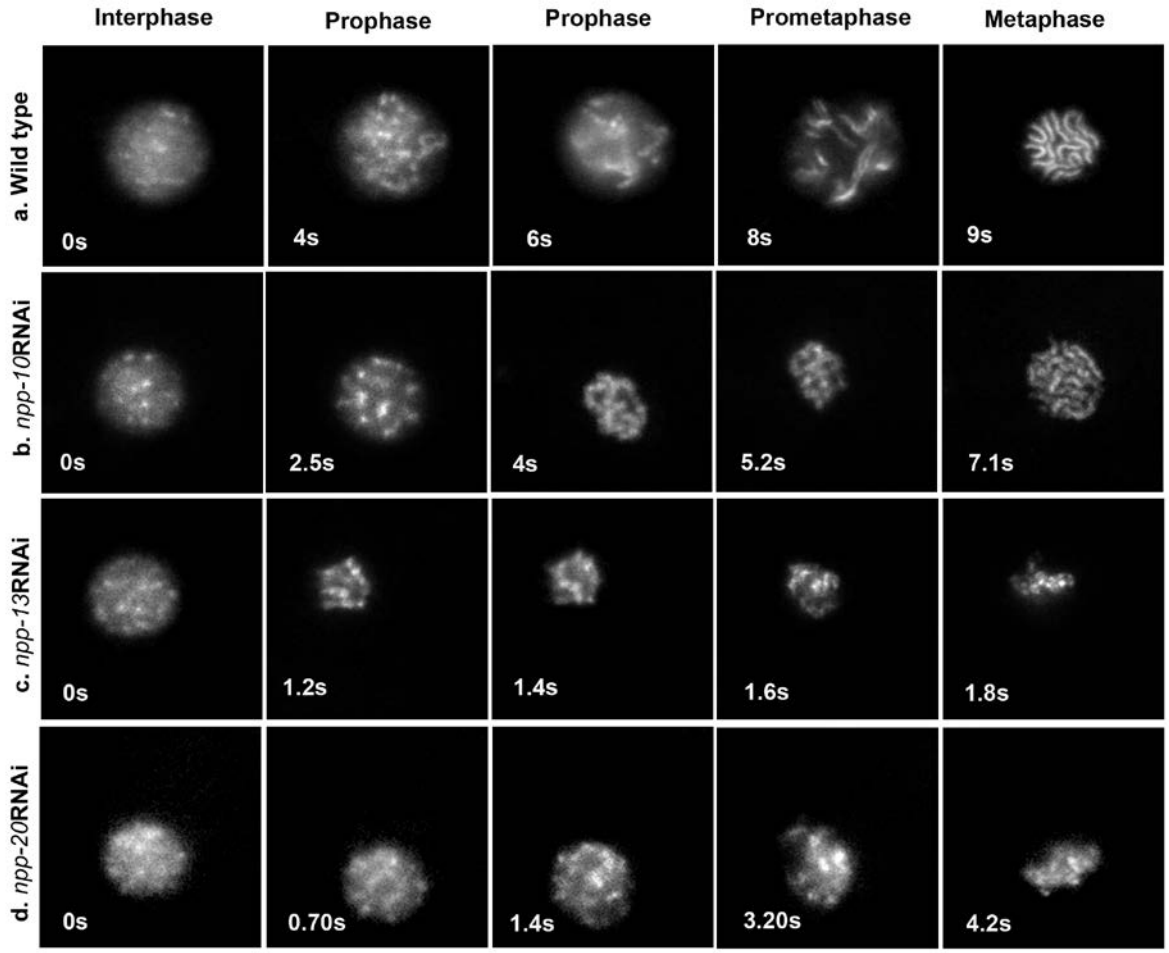

Supplemental material Figure S2: Knockdown of nucleoporins results in mitotic aberrations: GFP-channel stills of the progeny of control and *npp-RNAi* treated GFP-HCP-3 transgenic 2-cell embryos as indicated on the left margin. Approximate mitotic phase for each column is indicated at the top. Numbers represents the time in min with 0:00 at the start of mitosis. The images represent single sections from the middle of the image stack; compare movies 2-6. Metaphase plate in a) and b) are in frontview (centrosomal perspective) and in c) and d) in side view (perpendicular perspective).

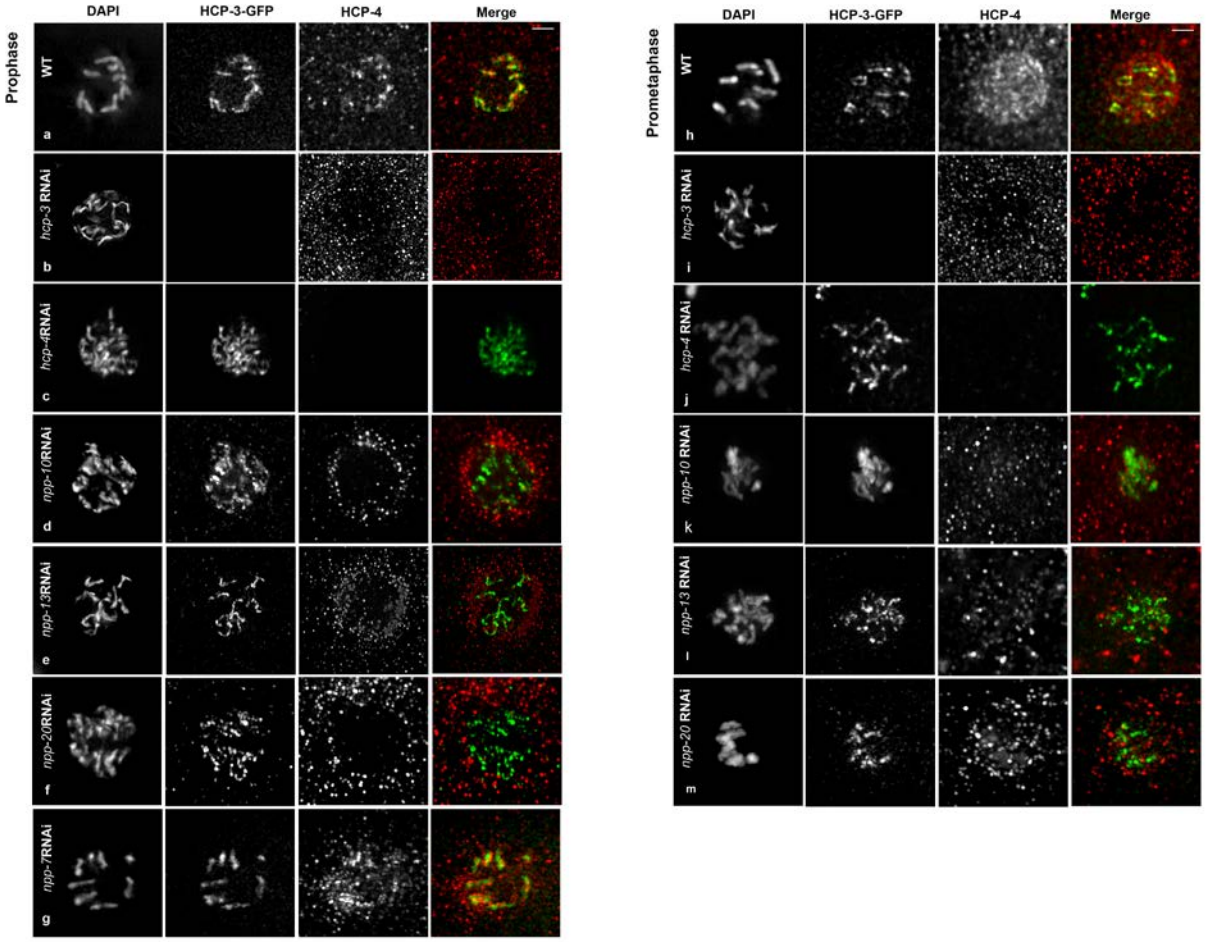

Supplemental material Figure S3. Knockdown of NPP-10, -13 and -20 results in nuclear exclusion of HCP-4 at prophase and loss of HCP-4 centromere binding at prometaphase: Fixed GFP-HCP-3 transgenic 2-cell embryos, treated by RNAi or untreated controls (wt), were stained by indirect immunofluorescence. Data are displayed as a projection of stacks of deconvolved images. GFP-antibodies (green), HCP-4 antisera (red), DAPI (blue). Single channels for DAPI, GFP-HCP-3 and HCP-4 in grey scale; merged GFP-HCP-3 (green) and HCP-4 (red) as indicated; left panel prophase nuclei: a) untreated wt control ; b) *HCP-3 RNAi;* c) *HCP-4 RNAi*; d) *npp-10 RNAi* ; e) *npp-13 RNAi* ; f) *npp-20 RNAi*; g) *npp-7 RNAi*; right panel prometaphase: h) untreated wt control ; i) *HCP-3 RNAi*; j) *HCP-4 RNAi*; k) *npp-10 RNAi* ; l) *npp-13 RNAi* ; m) *npp-20 RNAi*; Bar 4 μm.

Supplementary table S1

Table S1
a) HCP-3-GFP

sample n	n wt Chr eval	% wt Chr	n wt dl	% wt dl	n wt sl	% wt sl	n npp-10 Chr eval	% npp-10 Chr	n npp-10 dl	% npp-10 dl	n npp-10 sl	% npp10 sl	n npp-13 Chr eval	% npp-13 Chr	n npp-13 dl	% npp-13 dl	n npp-13 sl	% npp13 sl	n npp-20 Chr eval	% npp-20 Chr	n npp-20 dl	% npp-20 dl	n npp-20 sl	% npp-20 sl
1.00	8.00	100.00	7.00	87.50	1.00	12.50	1.00	100.00	0.00	0.00	1.00	100.00	4.00	100.00	0.00	0.00	4.00	100.00	7.00	100.00	2.00	28.57	5.00	71.43
2.00	4.00	100.00	4.00	100.00	0.00	0.00	1.00	100.00	0.00	0.00	1.00	100.00	1.00	100.00	1.00	100.00	0.00	0.00	4.00	100.00	1.00	25.00	3.00	75.00
3.00	11.00	100.00	10.00	90.91	1.00	9.10	2.00	100.00	1.00	50.00	1.00	50.00	3.00	100.00	1.00	33.33	2.00	66.67	5.00	100.00	0.00	0.00	5.00	100.00
4.00	11.00	100.00	11.00	100.00	0.00	0.00	1.00	100.00	0.00	0.00	1.00	100.00	6.00	100.00	2.00	33.33	4.00	66.67	9.00	100.00	4.00	44.44	5.00	55.56
5.00	10.00	100.00	10.00	100.00	0.00	0.00	3.00	100.00	1.00	33.00	2.00	66.70	5.00	100.00	2.00	40.00	3.00	60.00	3.00	100.00	0.00	0.00	3.00	100.00
6.00	11.00	100.00	10.00	90.91	1.00	9.10	4.00	100.00	0.00	0.00	4.00	100.00	6.00	100.00	2.00	33.33	4.00	66.67	7.00	100.00	4.00	57.14	3.00	42.86
7.00	10.00	100.00	10.00	100.00	0.00	0.00	3.00	100.00	0.00	0.00	3.00	100.00	4.00	100.00	2.00	50.00	2.00	50.00	7.00	100.00	4.00	57.14	3.00	42.86
8.00	11.00	100.00	11.00	100.00	0.00	0.00	9.00	100.00	7.00	77.80	2.00	22.00	3.00	100.00	0.00	0.00	3.00	100.00	6.00	100.00	0.00	0.00	6.00	100.00
9.00	10.00	100.00	10.00	100.00	0.00	0.00	2.00	100.00	2.00	30.00	0.00	0.00	4.00	100.00	2.00	50.00	2.00	50.00	5.00	100.00	0.00	0.00	5.00	100.00
10.00	11.00	100.00	10.00	90.91	1.00	9.10	6.00	100.00	2.00	20.00	4.00	100.00	6.00	100.00	1.00	16.67	5.00	83.33	5.00	100.00	3.00	60.00	2.00	40.00
11.00	8.00	100.00	8.00	100.00	0.00	0.00	3.00	100.00	3.00	37.50	0.00	0.00	5.00	100.00	1.00	20.00	4.00	80.00	3.00	100.00	1.00	33.33	2.00	66.67
12.00	11.00	100.00	11.00	100.00	0.00	0.00	6.00	100.00	1.00	16.70	5.00	83.30	4.00	100.00	2.00	50.00	2.00	50.00	3.00	100.00	0.00	0.00	3.00	100.00
13.00	9.00	100.00	8.00	88.89	1.00	11.11	1.00	100.00	0.00	0.00	1.00	100.00	5.00	100.00	3.00	60.00	2.00	40.00	6.00	100.00	5.00	83.33	1.00	16.67
14.00	10.00	100.00	10.00	100.00	0.00	0.00	1.00	100.00	0.00	0.00	1.00	100.00	5.00	100.00	1.00	16.67	4.00	66.67	7.00	100.00	5.00	71.43	2.00	28.57
15.00	11.00	100.00	10.00	90.91	1.00	9.10	1.00	100.00	0.00	0.00	1.00	25.00	7.00	100.00	3.00	42.86	4.00	57.14	2.00	100.00	0.00	100.00	2.00	100.00
16.00	7.00	100.00	7.00	100.00	0.00	0.00	3.00	100.00	1.00	33.00	2.00	66.70	7.00	100.00	2.00	28.57	5.00	71.43	7.00	100.00	4.00	57.14	3.00	42.86
17.00	9.00	100.00	9.00	100.00	0.00	0.00	2.00	100.00	0.00	0.00	2.00	100.00	5.00	100.00	2.00	33.33	3.00	50.00	2.00	100.00	0.00	0.00	2.00	100.00
18.00	10.00	100.00	8.00	80.00	2.00	20.00	1.00	100.00	1.00	33.00	0.00	0.00	3.00	100.00	2.00	66.67	1.00	33.33	7.00	100.00	5.00	71.43	2.00	28.57
19.00	11.00	100.00	11.00	100.00	0.00	0.00	2.00	100.00	0.00	0.00	2.00	100.00	4.00	100.00	2.00	50.00	2.00	50.00	6.00	100.00	0.00	0.00	6.00	100.00
Total n Chr	183.00		175.00		8.00		52.00		19.00		33.00		87.00		31.00		56.00		101.00		38.00		63.00	
Mean	9.63	100.00	9.21	95.79	0.42	4.21	2.74	100.00	1.00	17.42	1.74	70.24	4.58	100.00	1.63	38.15	2.95	60.10	5.32	100.00	2.00	36.26	3.32	69.00
SD	1.78		1.76	5.95	0.59	5.96	2.12		1.65	21.81	1.37	38.81	1.46		0.81	23.00	1.32	22.56	1.95		2.03	32.52	1.49	29.75

n npp-7 Chr eval	% npp-7 Chr	n npp-7 dl	% npp-7 dl	n npp-7 sl	%npp-7 sl	n npp-8 Chr eval	% npp-8 Chr	n npp-8 dl	% npp-8 dl	n npp-8 sl	% npp-8 sl	n npp-19 Chr eval	% npp-19 Chr	n npp-19 dl	% npp-19 dl	n npp-19 sl	% npp-19 sl
8.00	100.00	8.00	100.00	0.00	0.00	5.00	100.00	2.00	40.00	3.00	60.00	9.00	100.00	6.00	66.67	3.00	33.33
8.00	100.00	6.00	75.00	2.00	25.00	7.00	100.00	7.00	100.00	0.00	0.00	8.00	100.00	7.00	77.78	1.00	11.11
7.00	100.00	6.00	85.71	1.00	14.29	5.00	100.00	3.00	60.00	2.00	40.00	7.00	100.00	5.00	71.43	2.00	28.57
7.00	100.00	7.00	100.00	0.00	0.00	7.00	100.00	7.00	100.00	0.00	0.00	8.00	100.00	5.00	62.50	3.00	37.50
6.00	100.00	5.00	83.33	1.00	16.67	7.00	100.00	6.00	120.00	1.00	20.00	8.00	100.00	6.00	75.00	2.00	25.00
8.00	100.00	6.00	75.00	2.00	25.00	10.00	100.00	8.00	80.00	2.00	20.00	10.00	100.00	6.00	60.00	4.00	40.00
6.00	100.00	6.00	100.00	0.00	0.00	8.00	100.00	8.00	100.00	0.00	0.00	7.00	100.00	5.00	71.43	2.00	28.57
5.00	100.00	5.00	100.00	0.00	0.00	7.00	100.00	7.00	100.00	0.00	0.00	8.00	100.00	5.00	62.50	3.00	37.50
7.00	100.00	5.00	71.43	2.00	28.57	9.00	100.00	7.00	77.78	2.00	22.22	7.00	100.00	5.00	62.50	2.00	25.00
6.00	100.00	6.00	100.00	0.00	0.00	5.00	100.00	5.00	100.00	0.00	0.00	8.00	100.00	7.00	87.50	1.00	12.50
8.00	100.00	8.00	100.00	0.00	0.00	8.00	100.00	6.00	75.00	2.00	25.00	7.00	100.00	5.00	71.43	2.00	28.57
7.00	100.00	5.00	71.43	2.00	28.57	8.00	100.00	4.00	50.00	4.00	50.00	9.00	100.00	5.00	55.56	4.00	44.44
6.00	100.00	5.00	83.33	1.00	16.67	9.00	100.00	8.00	88.89	1.00	11.11	6.00	100.00	4.00	66.67	2.00	33.33
6.00	100.00	4.00	66.67	2.00	33.33	8.00	100.00	6.00	75.00	2.00	25.00	7.00	100.00	6.00	85.71	1.00	14.29
7.00	100.00	7.00	100.00	0.00	0.00	6.00	100.00	5.00	83.33	1.00	16.67	10.00	100.00	9.00	90.00	1.00	10.00
7.00	100.00	4.00	57.14	3.00	42.86	7.00	100.00	4.00	57.14	3.00	42.86	9.00	100.00	8.00	88.89	1.00	11.11
9.00	100.00	9.00	100.00	0.00	0.00	7.00	100.00	2.00	28.57	5.00	71.43	9.00	100.00	6.00	66.67	3.00	33.33
9.00	100.00	6.00	66.67	3.00	33.33	5.00	100.00	1.00	20.00	4.00	80.00	8.00	100.00	6.00	75.00	2.00	25.00
6.00	100.00	6.00	100.00	0.00	0.00	9.00	100.00	8.00	88.89	1.00	11.11	9.00	100.00	5.00	55.56	4.00	44.44
133.00		114.00		19.00		137.00		104.00		33.00		154.00		111.00		43.00	
7.00	100.00	6.00	85.71	1.00	14.29	7.21	100.00	5.47	76.03	1.74	26.07	8.11	100.00	5.84	71.20	2.26	27.56
1.08		1.30	14.55	1.08	14.55	1.47		2.19	26.35	1.48	24.27	1.07		1.18	10.56	1.02	11.00

	wt	npp-10	npp-13	npp-20	npp-7	npp-8	npp-19
% double line	95.79	17.42	38.15	36.26	85.71	76.03	71.20
SD	5.95	21.81	23.00	35.52	14.55	26.35	10.56

	wt	npp-10	npp-13	npp-20	npp-7	npp-8	npp-19
% single line	4.21	70.24	60.1	69	14.29	26.07	27.56
SD	5.96	39.72	22.56	29.75	14.55	24.27	11.00

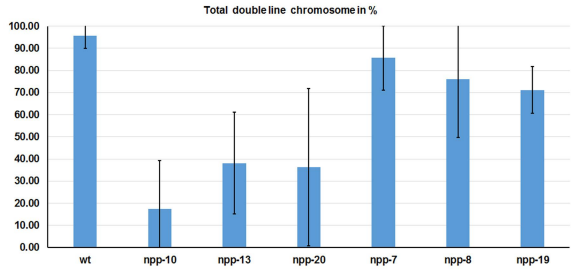

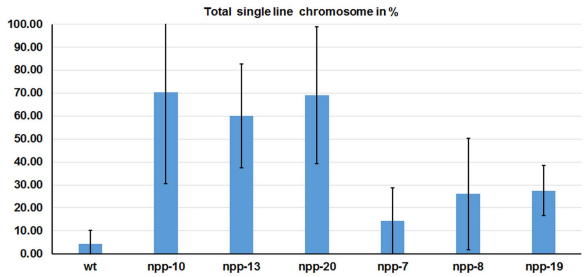

Supplementary Table S1a:

Quantification of centromere phenotypes following RNA knockdown: GFP-HCP-3 transgenic 2-cell embryos, treated by *npp* RNAi or untreated controls (wt), were stained with anti-GFP-antibodies and MAb 414. Each 19 two-cell embryos with cytologically distinct prometaphase chromosomes, lacking a nuclear envelope, were randomly chosen for evaluation. Distinct chromosomes with centromere resolution were counted as "double line" (dl) chromosomes, those who did not were counted as "single line" (sl) chromosomes. Data for wild type controls and *npp-10, -13, -20, -7, -8* and *-19* RNAi animals are listed in table S1a as total number of chromosomes evaluated (n Chr eval), number of double line chromosomes (n dl) and of single line chromosomes (n sl). In addition the number of dl and sl chromosomes was expressed as the fraction of all chromosome in percent. From these data the mean and standard deviation were calculated for each condition (small table above the graphs) and graphically displayed. Comparing wildtype with *npp* RNAi animals by two sample t-test assuming unequal variances confirmed the significance of our data for double line (*npp-10*: 1.574 E-12; *npp-13*: 0.308; *npp-20*: 3.297 E-07) and for single line (*npp-10*: 1.110 E-06; *npp-13*: 2.425 E-09; *npp-20*: 2.516 E-08) chromosomes.

Journal of Cell Science • Supplementary information

Table S1																		
b) KNL-2-GFP																		
sample n	n wt Chr eval	% wt Chr	n wt dl	% wt dl	n wt sl	% wt sl	n npp-10 Chr eval	% npp-10 Chr	n npp-10 dl	% npp-10 dl	n npp-10 sl	% npp-10 sl	n npp-13 Chr eval	% npp-13 Chr	n npp-13 Chr dl	% npp-13 dl	n npp-13 Chr sl	% npp-13 sl
1	11.00	100.00	7.00	63.64	4.00	36.36	1.00	100.00	0.00	0.00	1.00	100.00	5.00	100.00	0.00	100.00	5.00	0.00
2	11.00	100.00	4.00	36.36	7.00	63.64	1.00	100.00	0.00	0.00	1.00	100.00	3.00	100.00	0.00	100.00	3.00	0.00
3	11.00	100.00	10.00	90.91	1.00	9.09	1.00	100.00	1.00	100.00	0.00	0.00	5.00	100.00	1.00	20.00	4.00	80.00
4	11.00	100.00	11.00	100.00	0.00	0.00	2.00	100.00	2.00	100.00	0.00	0.00	7.00	100.00	1.00	14.29	6.00	85.71
5	10.00	100.00	11.00	100.00	0.00	0.00	4.00	100.00	1.00	25.00	3.00	75.00	7.00	100.00	4.00	57.14	3.00	42.86
6	11.00	100.00	10.00	90.91	1.00	9.09	4.00	100.00	1.00	25.00	3.00	75.00	6.00	100.00	0.00	0.00	6.00	100.00
7	11.00	100.00	10.00	90.91	1.00	9.09	2.00	100.00	1.00	50.00	1.00	50.00	3.00	100.00	0.00	0.00	3.00	100.00
8	11.00	100.00	11.00	100.00	0.00	0.00	5.00	100.00	4.00	80.00	1.00	20.00	4.00	100.00	2.00	50.00	2.00	50.00
9	11.00	100.00	10.00	90.91	1.00	9.09	6.00	100.00	0.00	0.00	6.00	100.00	5.00	100.00	0.00	0.00	5.00	100.00
10	11.00	100.00	10.00	90.91	1.00	9.09	2.00	100.00	2.00	100.00	0.00	0.00	6.00	100.00	2.00	33.33	4.00	66.67
11	11.00	100.00	8.00	72.73	3.00	27.27	7.00	100.00	2.00	28.57	5.00	71.43	6.00	100.00	1.00	16.67	5.00	83.33
12	11.00	100.00	9.00	81.82	2.00	18.18	2.00	100.00	2.00	100.00	0.00	0.00	5.00	100.00	0.00	0.00	5.00	100.00
13	11.00	100.00	8.00	72.73	3.00	27.27	1.00	100.00	0.00	0.00	1.00	100.00	5.00	100.00	4.00	80.00	1.00	20.00
14	11.00	100.00	10.00	90.91	1.00	9.09	1.00	100.00	1.00	100.00	0.00	0.00	3.00	100.00	0.00	0.00	3.00	0.00
15	11.00	100.00	10.00	90.91	1.00	9.09	3.00	100.00	0.00	0.00	3.00	100.00	5.00	100.00	1.00	20.00	4.00	80.00
16	11.00	100.00	7.00	63.64	4.00	36.36	3.00	100.00	1.00	33.33	2.00	66.67	6.00	100.00	3.00	50.00	3.00	50.00
17	11.00	100.00	9.00	81.82	2.00	18.18	0.00	100.00	0.00	0.00	0.00	0.00	6.00	100.00	3.00	50.00	3.00	50.00
18	11.00	100.00	8.00	72.73	3.00	27.27	2.00	100.00	0.00	0.00	2.00	100.00	4.00	100.00	1.00	25.00	3.00	75.00
19	11.00	100.00	10.00	90.91	1.00	9.09	2.00	100.00	1.00	50.00	1.00	50.00	4.00	100.00	2.00	50.00	2.00	50.00
Total n Chr	208.00		173.00		36.00		49.00		19.00		30.00		95.00		25.00		70.00	
Mean	10.95	100.00	9.11	82.78	1.89	17.22	2.58	100.00	1.00	41.68	1.58	53.06	5.00	100.00	1.32	35.08	3.68	59.66
SD	0.22		1.71	15.58	1.71	16.00	1.82		1.03	40.76	1.70	41.49	1.21		1.34	31.88	1.34	33.85

n npp-20 Chr eval	% npp-20 Chr	n npp-20 Chr dl	% npp-20 dl	n npp-20 Chr sl	% npp-20 sl	n npp-7 Chr eval	% npp-7 Chr	n npp-7 Chr dl	% npp-7 dl	n npp-7 Chr sl	% npp-7 sl
7.00	100.00	3.00	42.86	4.00	57.14	9.00	100.00	5.00	55.56	4.00	44.44
7.00	100.00	1.00	14.29	6.00	85.71	6.00	100.00	5.00	83.33	1.00	16.67
5.00	100.00	1.00	20.00	4.00	80.00	6.00	100.00	4.00	66.67	2.00	33.33
10.00	100.00	4.00	40.00	6.00	60.00	5.00	100.00	5.00	100.00	0.00	0.00
5.00	100.00	3.00	60.00	2.00	40.00	7.00	100.00	7.00	100.00	0.00	0.00
4.00	100.00	2.00	50.00	2.00	50.00	7.00	100.00	5.00	71.43	2.00	28.57
7.00	100.00	3.00	42.86	4.00	57.14	6.00	100.00	4.00	66.67	2.00	33.33
4.00	100.00	0.00	0.00	4.00	100.00	7.00	100.00	5.00	71.43	2.00	28.57
3.00	100.00	1.00	33.33	2.00	66.67	5.00	100.00	5.00	100.00	0.00	0.00
6.00	100.00	2.00	33.33	4.00	66.67	7.00	100.00	4.00	57.14	3.00	42.86
5.00	100.00	0.00	0.00	5.00	100.00	6.00	100.00	6.00	100.00	0.00	0.00
3.00	100.00	0.00	0.00	3.00	100.00	7.00	100.00	4.00	57.14	3.00	42.86
7.00	100.00	2.00	28.57	5.00	71.43	8.00	100.00	4.00	50.00	4.00	50.00
6.00	100.00	1.00	16.67	5.00	83.33	8.00	100.00	6.00	75.00	2.00	25.00
5.00	100.00	1.00	20.00	4.00	80.00	6.00	100.00	5.00	83.33	1.00	16.67
6.00	100.00	1.00	16.67	5.00	83.33	9.00	100.00	0.00	100.00	9.00	0.00
3.00	100.00	0.00	0.00	3.00	100.00	7.00	100.00	4.00	57.14	3.00	42.86
4.00	100.00	1.00	25.00	3.00	75.00	7.00	100.00	4.00	57.14	3.00	42.86
5.00	100.00	1.00	20.00	4.00	80.00	6.00	100.00	6.00	100.00	0.00	0.00
102.00		27.00		75.00		129.00		88.00		41.00	
5.37	100.00	1.42	24.40	3.95	75.60	6.79	100.00	4.63	76.42	2.16	23.58
1.72		1.14	17.30	1.19	17.30	1.10		1.38	18.20	2.08	18.20

	wt	npp-10	npp-13	npp-20	npp-7
% double line	82.78	41.68	35.08	24.4	76.42
SD	15.58	40.76	31.88	17.3	18.2

	wt	npp-10	npp-13	npp-20	npp-7
% single line	17.22	53.06	59.66	75.6	23.58
SD	16	41.49	33.85	17.3	18.2

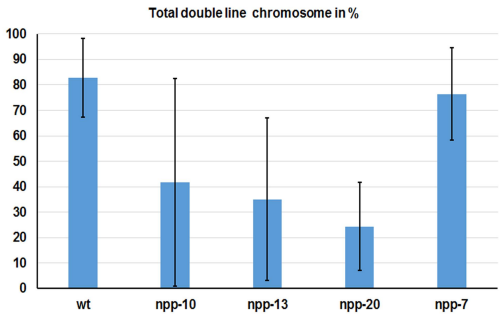

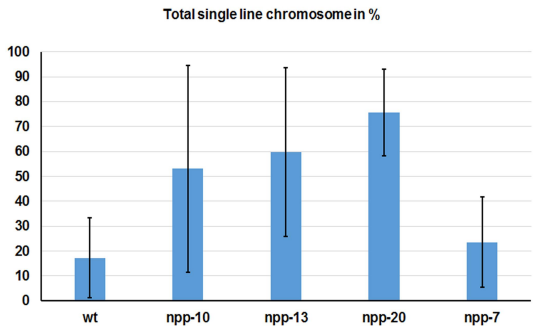

Supplementary Table S1b:

Quantification of centromere phenotypes following RNA knockdown: Data were collected from KNL-2-GFP transgenic embryos for wildtype and *npp-10-*, *npp-13-*, *npp-20-* and *npp-7-* RNAi and are displayed in table S1b and the corresponding graphic representation as described in table S1a.

Supplementary table S2

table S2a: wild type

a) control, HCP-4															
nucleus data															
n=1			n=2			n=3			n=4			n=5			
Stacks	mean	Mean -minimal pixel value	Stacks	mean	Mean -minimal pixel value	Stacks	mean	Mean -minimal pixel value	Stacks	mean	Mean -minimal pixel value	Stacks	mean	Mean -minimal pixel value	
1	30.067	12.497	1	38.801	19.121	1	42.913	25.343	1	33.027	20.857	1	28.19	10.43	
2	29.573	12.003	2	35.039	15.359	2	41.987	24.417	2	34	21.83	2	29.183	11.423	
3	29.688	12.118	3	43.158	23.478	3	43.097	25.527	3	36.444	24.274	3	30.147	12.387	
4	29.812	12.242	4	43.661	23.981	4	44.137	26.567	4	37.781	25.611	4	31.777	14.017	
5	30.081	12.511	5	43.636	23.956	5	46.73	29.16	5	38.374	26.204	5	35.253	17.493	
6	30.075	12.505	6	43.28	23.6	6	46.03	28.46	6	37.011	24.841	6	37.286	19.526	
7	29.818	12.248	7	45.049	25.369	7	44.163	26.593	7	36.128	23.958	7	37.949	20.189	
8	30.359	12.789	8	44.128	24.448	8	43.147	25.577	8	38.053	25.883	8	38.051	20.291	
9	31.088	13.518	9	44.756	25.076	9	42.917	25.347	9	30.321	18.151	9	37.462	19.702	
10	31.554	13.984	10	41.709	22.029	10	43.973	26.403	10	30.797	18.627	10	36.681	18.921	
11	32.032	14.462	11	41.421	21.741	11	47.403	29.833	11	31.053	18.883	11	34.465	16.705	
12	32.49	14.92	12	40.755	21.075	12	51.463	33.893	12	33.487	21.317	12	33.802	16.042	
13	33.273	15.703	13	36.516	16.836	13	51.677	34.107	13	36.358	24.188	13	34.564	16.804	
14	33.914	16.344	14	29.064	9.384	14	50.193	32.623	14	37.92	25.75	14	35.212	17.452	
15	34.138	16.568	15	29.118	9.438	15	51.443	33.873	15	38.818	26.648	15	35.315	17.555	
16	34.878	17.308	16	26.369	6.689	16	51.08	33.51	16	38.786	26.616	16	36.234	18.474	
17	35.878	18.308	17	27.153	7.473	17	51.613	34.043	17	37.968	25.798	17	38.44	20.68	
18	35.226	17.656	18	27.736	8.056	18	52.353	34.783	18	36.262	24.092	18	39.597	21.837	
19	34.307	16.737	19	29.805	10.125	19	52.353	34.783	19	35.182	23.012	19	39.092	21.332	
20	33.976	16.406	20	28.378	8.698	20	53.08	35.51	20	32.706	20.536	20	37.33	19.57	
21	34.997	17.427	21	28.032	8.352	21	51.887	34.317	21	31.374	19.204	21	35.685	17.925	
22	34.997	17.427	22	28.562	8.882	22	49.157	31.587	22	20.733	8.563	22	34.612	16.852	
Average	32.37368182	14.80368182		36.18754545	16.50754545		47.85436364	30.28436364		34.66286364	22.49286364		35.287591	17.52759091	
SD	2.169793651			7.034905431			3.882212953			4.086188381			3.044019		

control, HCP-4															
Cytoplasm data															
n=1			n=2			n=3			n=4			n=5			
Stacks	mean	Mean -minimal pixel value	Stacks	mean	Mean -minimal pixel value	Stacks	mean	Mean -minimal pixel value	Stacks	mean	Mean -minimal pixel value	Stacks	mean	Mean -minimal pixel value	
1	33.633	16.063	1	65.723	46.043	1	29.247	11.677	1	25.497	13.327	1	44.781	27.021	
2	36.417	18.847	2	63.491	43.811	2	29.397	11.827	2	25.155	12.985	2	45.186	27.426	
3	35.237	17.667	3	62.717	43.037	3	29.747	12.177	3	25.476	13.306	3	44.803	27.043	
4	30.267	12.697	4	61.863	42.183	4	29.159	11.589	4	25.524	13.354	4	45.523	27.763	
5	29.28	11.71	5	60.179	40.499	5	27.344	9.774	5	25.332	13.162	5	44.057	26.297	
6	29.73	12.16	6	58.402	38.722	6	25.381	7.811	6	24.963	12.793	6	42.243	24.483	
7	30.3	12.73	7	57.47	37.79	7	24.853	7.283	7	24.508	12.338	7	42.623	24.863	
8	35.247	17.677	8	56.839	37.159	8	24.509	6.939	8	24.642	12.472	8	46.11	28.35	
9	37.853	20.283	9	59.658	39.978	9	24.682	7.112	9	25.476	13.306	9	47.509	29.749	
10	37.117	19.547	10	60.018	40.338	10	26.364	8.794	10	26.385	14.215	10	44.081	26.321	
11	36.193	18.623	11	59.506	39.826	11	26.934	9.364	11	26.695	14.525	11	43.216	25.456	
12	33.663	16.093	12	58.863	39.183	12	26.066	8.496	12	27.337	15.167	12	47.574	29.814	
13	32.633	15.063	13	55.708	36.028	13	26.093	8.523	13	27.225	15.055	13	49.427	31.667	
14	34.653	17.083	14	53.387	33.707	14	26.574	9.004	14	27.043	14.873	14	47.379	29.619	
15	37.793	20.223	15	52.179	32.499	15	26.742	9.172	15	26.364	14.194	15	46.603	28.843	
16	37.69	20.12	16	52.179	32.499	16	27.028	9.458	16	26.524	14.354	16	48.273	30.513	
17	34.273	16.703	17	51.634	31.954	17	27.13	9.56	17	27.503	15.333	17	46.273	28.513	
18	32.647	15.077	18	51.47	31.79	18	26.694	9.124	18	28.572	16.402	18	44.98	27.22	
19	32.717	15.147	19	53.518	33.838	19	26.358	8.788	19	37.888	25.718	19	45.239	27.479	
20	33.277	15.707	20	56.964	37.284	20	26.358	8.788	20	36.364	24.194	20	45.239	27.479	
21	34.98	17.41	21	59.887	40.207	21	28.597	11.027	21	36.273	24.103	21	44.781	27.021	
22	36.407	18.837	22	64.708	45.028	22	28.255	10.685	22	35.316	23.146	22	45.307	27.547	
Average	34.18213636	16.61213636		58.0165	38.3365		26.97781818	9.407818182		28.00281818	15.83281818		45.5094091	27.74940909	
SD	2.585613103			4.21319821			1.49744287			4.125499371			1.75063284		

control, HCP-4			
Nucleus vs Cytoplasm			
Stacks	nucleus	cytoplasm	ratio
1	14.8036	16.61	0.891246237
2	16.508	38.3	0.431018277
3	30.284	9.4	3.221702128
4	22.49	15.8	1.423417722
5	17.5276	27.749	0.631647987
Average			1.31980647
SD			1.007483281

table S2b: *npp-10* RNAi

b) NPP-10 HCP-4																	
nucleus data																	
n=1			n=2			n=3			n=4			n=5					
Stacks	mean	Mean -minimal pixel value	Stacks	mean	Mean -minimal pixel value	Stacks	mean	Mean -minimal pixel value	Stacks	mean	Mean -minimal pixel value	Stacks	mean	Mean -minimal pixel value			
1	20.718	5.308	1	30.329	6.409	1	32.446	3.136	1	43.458	24.966	1	58.914	42.924			
2	19.111	3.701	2	30.879	6.959	2	31.488	2.178	2	43.662	25.17	2	57.982	41.992			
3	17.598	2.188	3	38.978	15.058	3	29.825	0.515	3	44.558	26.066	3	57.145	41.155			
4	16.998	1.588	4	35.547	11.627	4	39.012	9.702	4	44.562	26.07	4	56.52	40.53			
5	17.95	2.54	5	28.36	4.44	5	37.917	8.607	5	45.442	26.95	5	55.643	39.653			
6	19.468	4.058	6	26.539	2.619	6	37.962	8.652	6	46.338	27.846	6	55.348	39.358			
7	20.595	5.185	7	27.029	3.109	7	39.296	9.986	7	48.012	29.52	7	54.896	38.906			
8	21.189	5.779	8	25.527	1.607	8	39.208	9.898	8	49.358	30.866	8	54.407	38.417			
9	21.009	5.599	9	29.8	5.88	9	37.579	8.269	9	49.95	31.458	9	54.059	38.069			
10	20.593	5.183	10	24.734	0.814	10	36.312	7.002	10	47.388	28.896	10	53.937	37.947			
11	20.211	4.801	11	25.274	1.354	11	31.4	2.09	11	45.246	26.754	11	54.235	38.245			
12	20.125	4.715	12	24.053	0.133	12	31.4	2.09	12	45.196	26.704	12	54.045	38.055			
13	20.009	4.599	13	24.308	0.388	13	31.4	2.09	13	45.55	27.058	13	53.742	37.752			
14	19.539	4.129	14	25.095	1.175	14	30.067	0.757	14	46.396	27.904	14	53.376	37.386			
15	18.939	3.529	15	24.351	0.431	15	31.25	1.94	15	49.442	30.95	15	52.606	36.616			
16	17.38	1.97	16	24.892	0.972	16	32.679	3.369	16	42.179	23.687	16	51.588	35.598			
17	15.855	0.445	17	25.192	1.272	17	30.3	0.99	17	41.004	22.512	17	50.498	34.508			
18	19.257	3.847	18	30.869	6.949	18	34.312	5.002	18	41.004	22.512	18	50.213	34.223			
19	19.207	3.797	19	30.431	6.511	19	30.288	0.978	19	45.192	26.7	19	49.253	33.263			
20	19.457	4.047	20	30.7	6.78	20	30.875	1.565	20	38.779	20.287	20	48.457	32.467			
21	19.239	3.829	21	29.987	6.067	21	30.038	0.728	21	38.588	20.096	21	47.371	31.381			
22	19.139	3.729	22	30.061	6.141	22	30.292	0.982	22	37.2	18.708	22	45.172	29.182			
Average	19.254	3.843909091		28.31522727	4.395227273		44.47745455	4.114818182		33.4248182	25.98545455		53.15486364	37.16486364			
SD	1.3434			3.800695127			3.447463675			3.43906652			3.411475411				

NPP-10 HCP-4																	
Cytoplasm data																	
n=1			n=2			n=3			n=4			n=5					
Stacks	mean	Mean -minimal pixel value	Stacks	mean	Mean -minimal pixel value	Stacks	mean	Mean -minimal pixel value	Stacks	mean	Mean -minimal pixel value	Stacks	mean	Mean -minimal pixel value			
1	41.754	26.344	1	40.189	16.269	1	44.33	15.02	1	57.609	39.117	1	57.683	41.693			
2	41.957	26.547	2	38.623	14.703	2	44.428	15.118	2	57.954	39.462	2	58.928	42.938			
3	41.804	26.394	3	38.75	14.83	3	44.002	14.692	3	57.427	38.935	3	60.226	44.236			
4	41.898	26.488	4	37.61	13.69	4	44.292	14.982	4	65.456	46.964	4	62.335	46.345			
5	41.511	26.101	5	37.995	14.075	5	43.986	14.676	5	69.023	50.531	5	64.407	48.417			
6	41.083	25.673	6	39.912	15.992	6	42.388	13.078	6	73.907	55.415	6	66.747	50.757			
7	39.363	23.953	7	39.444	15.524	7	41.844	12.534	7	72.613	54.121	7	69.176	53.186			
8	38.489	23.079	8	41.225	17.305	8	42.018	12.708	8	73.479	54.987	8	71.778	55.788			
9	38.965	23.555	9	41.826	17.906	9	42.018	12.708	9	67.14	48.648	9	74.679	58.689			
10	38.498	23.088	10	41.154	17.234	10	42.038	12.728	10	66.244	47.752	10	77.833	61.843			
11	37.339	21.929	11	39.65	15.73	11	43.402	14.092	11	69.341	50.849	11	79.489	63.499			
12	37.159	21.749	12	39.949	16.029	12	44.276	14.966	12	67.761	49.269	12	82.122	66.132			
13	36.335	20.925	13	39.26	15.34	13	44.784	15.474	13	63.134	44.642	13	83.805	67.815			
14	36.365	20.955	14	39.956	16.036	14	45.58	16.27	14	68.112	49.62	14	83.95	67.96			
15	36.554	21.144	15	39.755	15.835	15	45.34	16.03	15	64.465	45.973	15	85.09	69.1			
16	36.074	20.664	16	39.914	15.994	16	44.974	15.664	16	60.653	42.161	16	74.421	58.431			
17	35.698	20.288	17	39.419	15.499	17	42.426	13.116	17	61.796	43.304	17	73.959	57.969			
18	35.307	19.897	18	38.157	14.237	18	41.124	11.814	18	57.075	38.583	18	71.643	55.653			
19	35.457	20.047	19	38.843	14.923	19	42.138	12.828	19	57.557	39.065	19	71.606	55.616			
20	35.711	20.301	20	38.238	14.318	20	41.972	12.662	20	65.903	47.411	20	72.882	56.892			
21	35.674	20.264	21	38.061	14.141	21	41.02	11.71	21	55.599	37.107	21	70.611	54.621			
22	34.883	19.473	22	38.066	14.146	22	40.23	10.92	22	64.874	46.382	22	70.018	54.028			
Average	38.085364	22.67536364		39.36345455	15.44345455		43.11863636	13.80863636		64.41463636	45.92263636		71.9721818	55.98218182			
SD	2.48757671			1.112234186			1.506832486			5.486705358			7.89422863				

NPP-10, HCP-4			
Nucleus vs Cytoplasm			
Stacks	nucleus	cytoplasm	ratio
1	3.84	22.67	0.169386855
2	4.39	15.44	0.284326425
3	4.11	13.8	0.297826087
4	25.98	45.9	0.566013072
5	37.16	55.98	0.663808503
Average			**0.396272188**
SD			**0.186594797**

table S2c: *npp-13* RNAi

c) NPP-13 HCP-4															
nucleus data															
n=1			n=2			n=3			n=4			n=5			
Stacks	mean	Mean -minimal pixel value	Stacks	mean	Mean -minimal pixel value	Stacks	mean	Mean -minimal pixel value	Stacks	mean	Mean -minimal pixel value	Stacks	mean	Mean -minimal pixel value	
1	50.647	33.077	1	41.959	16.159	1	37.61	18.03	1	44.063	22.753	1	21.425	8.515	
2	51.927	34.357	2	42.024	16.224	2	37.387	17.807	2	43.616	22.306	2	21.476	8.566	
3	50.833	33.263	3	41.976	16.176	3	36.346	16.766	3	44.553	23.243	3	21.916	9.006	
4	49.903	32.333	4	40.176	14.376	4	34.775	15.195	4	45.833	24.523	4	22.423	9.513	
5	50.227	32.657	5	40.415	14.615	5	33.181	13.601	5	43.472	22.162	5	22.318	9.408	
6	49.953	32.383	6	39.035	13.235	6	31.055	11.475	6	43.202	21.892	6	22.888	9.978	
7	49.34	31.77	7	38.167	12.367	7	30.442	10.862	7	44.909	23.599	7	24.606	11.696	
8	48.8	31.23	8	37.098	11.298	8	30.681	11.101	8	45.965	24.655	8	25.604	12.694	
9	46.6	29.03	9	36.219	10.419	9	31.431	11.851	9	43.785	22.475	9	25.512	12.602	
10	44.497	26.927	10	37.146	11.346	10	32.247	12.667	10	42.505	21.195	10	25.556	12.646	
11	44.243	26.673	11	38.041	12.241	11	31.714	12.134	11	41.677	20.367	11	25.493	12.583	
12	43.807	26.237	12	40.044	14.244	12	31.835	12.255	12	41.02	19.71	12	24.701	11.791	
13	45.077	27.507	13	41.515	15.715	13	33.28	13.7	13	40.846	19.536	13	23.484	10.574	
14	45.9	28.33	14	41.32	15.52	14	34.536	14.956	14	40.505	19.195	14	21.758	8.848	
15	47.057	29.487	15	41.643	15.843	15	34.519	14.939	15	40.25	18.94	15	20.28	7.37	
16	46.323	28.753	16	42.363	16.563	16	34.871	15.291	16	40.384	19.074	16	19.619	6.709	
17	45.773	28.203	17	43.607	17.807	17	34.819	15.239	17	39.813	18.503	17	19.015	6.105	
18	43.787	26.217	18	44.404	18.604	18	35.868	16.288	18	37.646	16.336	18	18.834	5.924	
19	42.483	24.913	19	44.374	18.574	19	36.299	16.719	19	38.795	17.485	19	18.585	5.675	
20	42.907	25.337	20	40.613	14.813	20	36.893	17.313	20	39.917	18.607	20	17.996	5.086	
21	46.933	29.363	21	39.669	13.869	21	36.154	16.574	21	40.699	19.389	21	17.962	5.052	
22	51.493	33.923	22	39.685	13.885	22	35.78	16.2	22	40.866	19.556	22	18.101	5.191	
Average	47.205	29.635		40.52240909	14.72240909		34.16922727	14.58922727		42.01459091	20.70459091		21.79781818	8.887818182	
SD	2.91069511			2.23072081			2.236471733			2.245641894			2.646278513		

NPP-13 HCP-4															
Cytoplasm data															
n=1			n=2			n=3			n=4			n=5			
Stacks	mean	Mean -minimal pixel value	Stacks	mean	Mean -minimal pixel value	Stacks	mean	Mean -minimal pixel value	Stacks	mean	Mean -minimal pixel value	Stacks	mean	Mean -minimal pixel value	
1	49.267	31.697	1	49.813	24.013	1	53.616	32.306	1	50.631	29.321	1	25.223	12.313	
2	55.277	37.707	2	48.561	22.761	2	54.553	33.243	2	54.662	33.352	2	24.886	11.976	
3	46.953	29.383	3	57.206	31.406	3	55.833	34.523	3	59.068	37.758	3	27.08	14.17	
4	58.737	41.167	4	57.611	31.811	4	53.472	32.162	4	63.99	42.68	4	32.528	19.618	
5	49.267	31.697	5	57.667	31.867	5	53.202	31.892	5	69.376	48.066	5	35.006	22.096	
6	60.483	42.913	6	59.024	33.224	6	54.909	33.599	6	75.121	53.811	6	39.467	26.557	
7	62.89	45.32	7	68.783	42.983	7	55.965	34.655	7	79.975	58.665	7	38.032	25.122	
8	59.583	42.013	8	66.741	40.941	8	53.785	32.475	8	84.727	63.417	8	37.587	24.677	
9	58.197	40.627	9	65.126	39.326	9	52.505	31.195	9	87.758	66.448	9	38.299	25.389	
10	57.68	40.11	10	64.4	38.6	10	51.677	30.367	10	88.591	67.281	10	38.436	25.526	
11	58.333	40.763	11	62.794	36.994	11	51.02	29.71	11	68.068	46.758	11	37.516	24.606	
12	55.007	37.437	12	60.878	35.078	12	50.846	29.536	12	67.861	46.551	12	35.964	23.054	
13	52.28	34.71	13	60.865	35.065	13	40.505	19.195	13	66.311	45.001	13	34.225	21.315	
14	51.777	34.207	14	59.552	33.752	14	40.25	18.94	14	64.561	43.251	14	32.602	19.692	
15	52.617	35.047	15	78.952	53.152	15	40.384	19.074	15	64.561	43.251	15	31.425	18.515	
16	51.813	34.243	16	58.976	33.176	16	39.813	18.503	16	62.904	41.594	16	30.589	17.679	
17	51.117	33.547	17	56.974	31.174	17	37.646	16.336	17	60.162	38.852	17	30.387	17.477	
18	49.237	31.667	18	52.509	26.709	18	38.795	17.485	18	56.141	34.831	18	30.194	17.284	
19	49.81	32.24	19	57.77	31.97	19	39.917	18.607	19	52.235	30.925	19	28.994	16.084	
20	49.487	31.917	20	53.22	27.42	20	40.699	19.389	20	48.912	27.602	20	27.726	14.816	
21	49.797	32.227	21	58.07	32.27	21	40.866	19.556	21	47.503	26.193	21	26.651	13.741	
22	40.46	22.89	22	55.491	29.691	22	39.866	18.556	22	47.821	26.511	22	25.661	12.751	
Average	53.184955	35.61495455		59.59013636	33.79013636		47.27836364	25.96836364		64.58814	43.27813636		32.203545	19.29354545	
SD	5.1856851			6.49852915			6.895195749			12.2554			4.7162052		

NPP_13, HCP-4			
Nucleus vs Cytoplasm			
Stacks	nucleus	cytoplasm	ratio
1	29.63	35.6	0.832303371
2	14.72	33.79	0.435631844
3	14.6	26	0.561538462
4	20.7	43.3	0.478060046
5	8.88	19.29	0.460342146
Average			0.553575174
SD			0.14564229

Supplementary table 2

Quantification of the nuclear to cytoplasmic ratio of HCP-4 staining in prophase embryos: Embryos from wild type and RNAi knockdown animals were double-stained for HCP-4 and the nuclear pore complex (MAb 414) and recorded as stacks of 22 images. Five randomly chosen prophase cells were evaluated for each condition. For each section of the stacks the mean intensity of HCP-4 staining in the nuclear (delineated by MAb414) and in an adjacent cytoplasmic region of same size was determined, both corrected for background by subtracting the minimal pixel intensity of the whole stack (table S2a for wild type, S2b for *npp-10* RNAi and S2c for *npp-13* RNAi). Using these data the mean intensity for nuclear or cytoplasmic compartment in the whole stack was determined and used to calculate the nucleus/cytoplasmic ratio of HCP-4 for the given cell (small tables in S2a-c). The mean and standard deviation of all five cells was graphically displayed in figure 5 as the nuclear/cytoplasmic ratio of HCP-4 staining for a given condition.

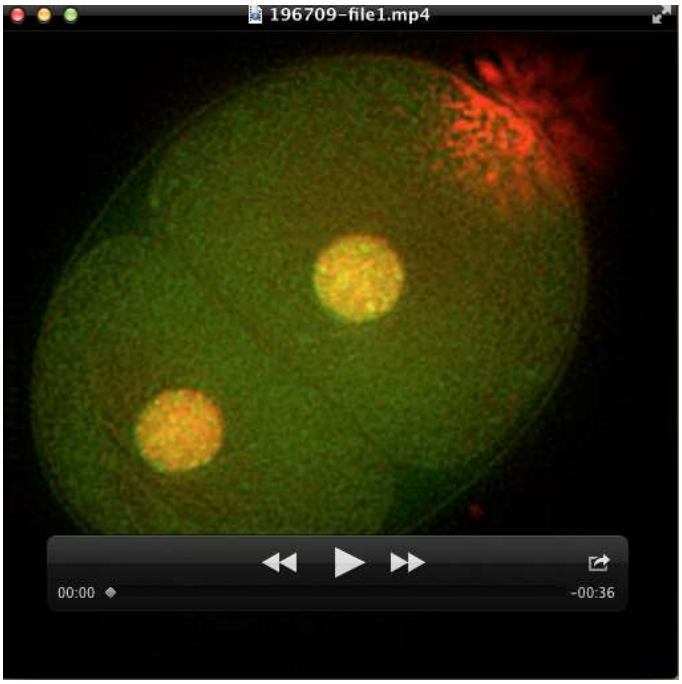

Movie 1: Centromere formation in a *C. elegans* 2-cell wt embryo visualized by KNL2 live imaging: GFP-KNL-2 (green) and histone H2A (red) double stained embryos were recorded by image restoration microscopy. The slightly larger AB-cell (right/upper) is more advanced than the P- cell (left/lower); however both cells pass a full mitosis. Compare supplemental figure 1.

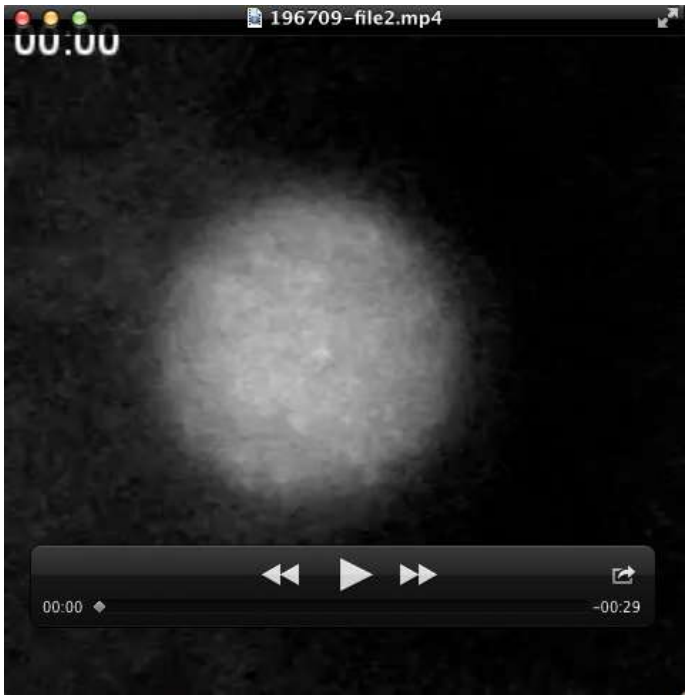

Movie 2: Centromere formation in a *C. elegans* 2-cell wt embryo visualized by HCP3 live imaging GFP-HCP-3 (green) transgenic embryos were recorded by image restoration microscopy. Shown is an AB-cell nucleus that passes a full mitosis. Compare figure 1.

Movie 3: Centromere formation in a *C. elegans* 2-cell *npp-7*RNAi embryo visualized by HCP-3 live imaging GFP-HCP-3 (green) transgenic embryos were recorded by image restoration microscopy. The slightly more advanced AB-cell of the embryo shown is at the bottom. Note loss of chromosomes during anaphase.

Movie 4: Centromere formation in a *C. elegans* 2-cell *npp-10*RNAi embryo visualized by HCP-3 live imaging GFP-HCP-3 (green) transgenic embryos were recorded by image restoration microscopy. Shown is an AB-cell nucleus that does not fully resolve anaphase bridges between separating chromosomal complements. Compare supplemental figure 2.

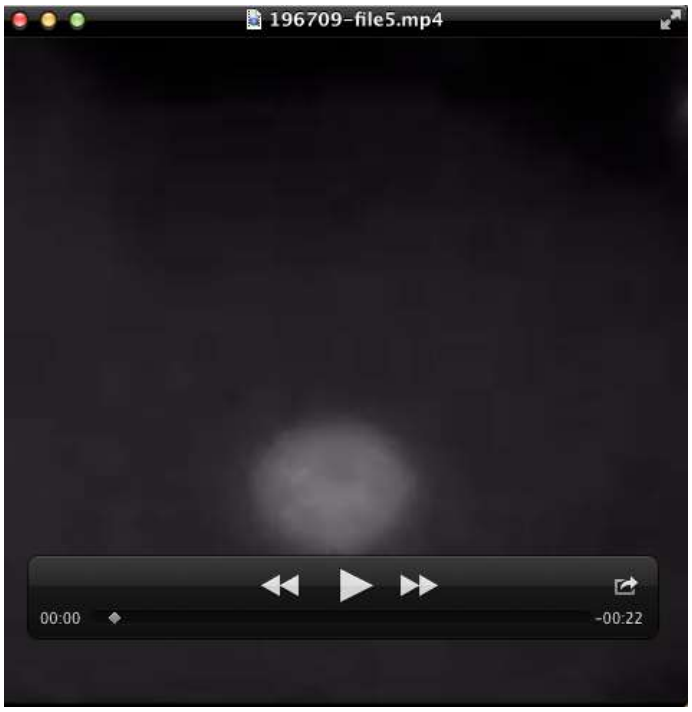

Movie 5: Centromere formation in a *C. elegans* 2-cell *npp-13*RNAi embryo visualized by HCP-3 live imaging GFP-HCP-3 (green) transgenic embryos were recorded by image restoration microscopy. The slightly more advanced AB-cell of the embryo shown is at the lower right. Note loss of chromosomal material during anaphase. Compare supplemental figure 2.

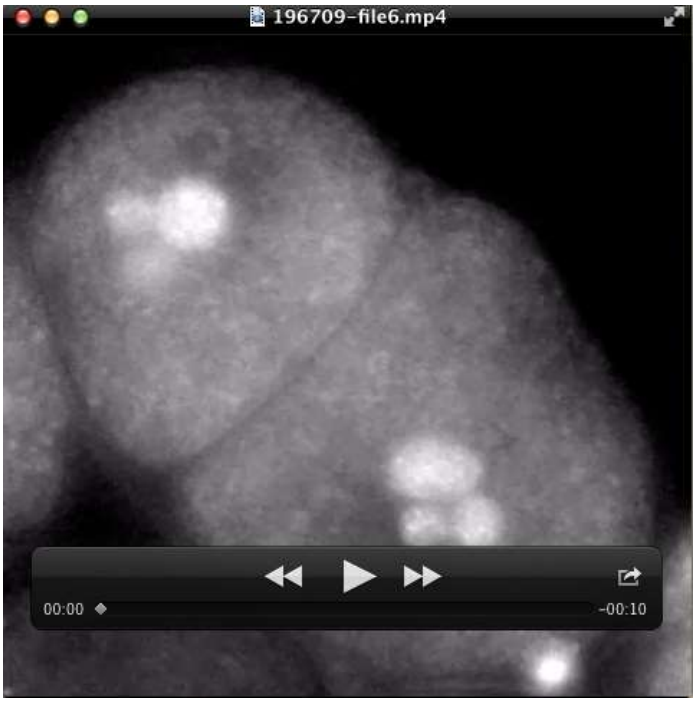

Movie 6. Centromere formation in a *C. elegans* 2-cell *npp-19*RNAi embryo visualized by HCP-3 live imaging GFP-HCP-3 (green) transgenic embryos were recorded by image restoration microscopy. The two cell embryo shown (AB at the lower right) shows a fragmented nucleus from the beginning. Note that despite the strong chromosomal abnormalities the centromere segregation still takes place rather normally.